From the computer to the laboratory: materials discovery and design using first-principles calculations

J Mater Sci (2012) 47:7317–7340
DOI 10.1007/s10853-012-6424-0

FIRST PRINCIPLES COMPUTATIONS

From the computer to the laboratory: materials discovery and design using first-principles calculations

Geoffroy Hautier · Anubhav Jain · Shyue Ping Ong

Received: 18 January 2012 / Accepted: 17 March 2012 / Published online: 10 May 2012

Abstract The development of new technological materials has historically been a difficult and time-consuming task. The traditional role of computation in materials design has been to better understand existing materials. However, an emerging paradigm for accelerated materials discovery is to design new compounds *in silico* using first-principles calculations, and then perform experiments on the computationally designed candidates. In this paper, we provide a review of ab initio computational materials design, focusing on instances in which a computational approach has been successfully applied to propose new materials of technological interest in the laboratory. Our examples include applications in renewable energy, electronic, magnetic and multiferroic materials, and catalysis, demonstrating that computationally guided materials design is a broadly applicable technique. We then discuss some of the common features and limitations of successful theoretical predictions across fields, examining the different ways in which first-principles calculations can guide the final experimental result. Finally, we present a future outlook in which we expect that new models of computational search, such as high-throughput studies, will play a greater role in guiding materials advancements.

G. Hautier (✉)
Institute of Condensed Matter and Nanosciences (IMCN)-Nanoscopic Physics (NAPS), Université Catholique de Louvain, Louvain-la-Neuve, Belgium
e-mail: geoffroy.hautier@uclouvain.be

A. Jain
Computational Research Division, Lawrence Berkeley National Laboratory, Berkeley, CA, USA

S. P. Ong
Department of Materials Science and Engineering, Massachusetts Institute of Technology, Cambridge, MA, USA

Introduction

There is a great need for new methods to accelerate materials design. Many major industries depend on materials advancements to bring improved technologies to market. Often, these technological challenges relate to societal problems, such as cleanly generating and using energy, that are currently in need of materials breakthroughs within short time frames.

However, materials innovations rarely appear overnight. Even after a new material demonstrates success in the laboratory, it takes about twenty additional years before its widespread adoption, largely due to the difficulties in building production capacities and lowering manufacturing costs from initial laboratory results [1]. It is therefore necessary to identify promising materials early on so that scale-up can begin as soon as possible. In addition, it is important to better understand the strengths and weaknesses of potential materials candidates early in the design process, as this helps avoid costly and time-consuming materials optimization down the road.

In recent years, ab initio or first-principles computations (i.e., based on solving the fundamental equations of quantum mechanics) have become ubiquitous in materials science, and it is nowadays hard to find a material of scientific interest that has not been studied computationally. The most popular approach to first-principles computations is currently by far density functional theory (DFT). Although the theoretical roots of modern DFT trace back to Hohenberg–Kohn theorems of 1964 [2], the last two decades of DFT research have been particularly important to materials design due to more accurate treatments of exchange and correlation effects of electrons, more powerful computational resources available to materials researchers, more efficient numerical algorithms, and the

introduction of several user-friendly commercial and open-source software packages for performing DFT computations [3–5].

Using a computational approach to help design new materials offers several benefits that are complementary to traditional experimental-based materials discovery. One key advantage of computations is the level of control they offer compared to experiments. For example, it is often trivial in calculations to simulate the effects of chemical substitutions or lattice strain, but achieving those same conditions experimentally could take many months of painstaking laboratory work. In addition, characterizing a material's fundamental properties is often quicker with computations compared to experiment while still retaining excellent or acceptable accuracy. This is most apparent in recent high-throughput DFT studies in which properties of thousands of materials have been calculated in relatively short time frames, opening up the possibility for an informatics-based approach to materials design. These advantages have now made computations an effective virtual laboratory for designing materials *in silico* prior to time-consuming and expensive laboratory work.

In this review, we highlight several examples where first-principles calculations have directly *predicted* materials with promising properties. In some of these cases, the suggested compounds were previously unknown, and the compound was in essence completely designed within a computer. In all cases reviewed here, the calculated results were subsequently verified by experimental measurements. By focusing on such predictive studies, we have left out many excellent studies where first-principles computations have greatly advanced our understanding of known materials; many such examples can be found in previous reviews [6, 7]. This work does not claim to be exhaustive and our goal in selecting examples has been to clearly demonstrate the capability of state-of-the-art calculations as a tool for rational and accelerated materials design in a broad number of applications, and to examine the typical challenges faced by researchers when making ab initio predictions.

The outline of this paper is as follows. The second section "Ab initio methods" serves as a technical introduction to ab initio computations and the materials properties that can presently be computed. The third section "Compound and crystal structure prediction" deals with the topic of crystal structure prediction and its role in the discovery of new materials. The fourth section "Case studies" present examples of materials design led by first-principles calculations in the fields of energy, catalysis, and electronic and magnetic materials. Finally, the fifth section "Status, challenges and future of computational materials discovery and design" provides a perspective on the role of first-principles computations in accelerating materials design and the sixth section "Conclusion" provides concluding remarks.

Ab initio methods

Because this review is about ab initio computational materials design, it behooves us to provide at least a brief description of the current state of ab initio methodological development. However, the literature on first-principles methods is vast and providing a comprehensive overview is outside the scope of this review. We will thus attempt to only provide a sufficiently broad outline of the general concepts pertinent to the applications discussed in subsequent sections, and the interested reader is pointed to the many excellent books [8] and reviews on ab initio methods [9–11]. The reader with expertise in first-principles methods can easily skip this section and turn directly to the section "Compound and crystal structure prediction" on compound and crystal structure prediction or to the case studies in section "Case studies".

A calculation is said to be ab initio (or from first-principles) if it relies on the fundamental laws of quantum physics without additional assumptions or special models. For the prediction of many materials properties, such a calculation generally involves studying a system of N electrons in an external potential and finding the solution to the many-body time-independent Schrödinger equation:

$$\left[-\frac{\hbar^2}{2m}\nabla^2 + V(\mathbf{r_1},\ldots,\mathbf{r_N})\right]\psi(\mathbf{r_1},\ldots,\mathbf{r_N}) = \epsilon\psi(\mathbf{r_1},\ldots,\mathbf{r_N}) \quad (1)$$

where $\hbar$ is Planck's constant, V is the potential (external and from the interaction between electrons), ψ is the many-body wavefunction, ϵ is the energy, and the $\mathbf{r_1},\ldots,\mathbf{r_N}$ represents the coordinates of the N electrons in the system.

Despite its deceptively simple analytic form, solving the Schrödinger equation is intractable for all but the simplest of systems, and we are thus forced to resort to various approximations to the exact solution. For solid-state applications (and also many molecular applications), the most widely used framework for finding approximate solutions to the Schrödinger equation is DFT.

DFT

DFT has its foundation in the Hohenberg–Kohn (H–K) theorem [2], which states that (i) all ground-state properties of a system, including the total energy, are some functional of the ground-state charge density; and (ii) the correct ground-state charge density minimizes the energy functional, i.e.,

$$E[n] = T[n] + U[n] + \int V(\mathbf{r})n(\mathbf{r})d^3\mathbf{r} \quad (2)$$

where n is the charge density, $\mathbf{r}$ is the position, E is the total energy, T is the kinetic energy, V is the potential energy

from the external field (typically due to the positively charged nuclei of the crystal), and U is the electron–electron interaction energy.

The H–K theorem implies that the ground-state for any system can be determined by varying the charge density until the global minimum in the energy functional is found. Thus, the complex problem of solving the many-body Schrödinger equation of N electrons with $3N$ spatial coordinates is reduced to a simpler (though still difficult) problem based on the charge density of 3 spatial coordinates. However, while the H–K theorem guarantees in principle a correspondence between the ground-state charge density and energy, the true functional relating the charge density to the energy is unknown.

The variational problem of minimizing the energy functional is typically solved by considering the so-called Kohn–Sham (K–S) equations [12] of an auxiliary non-interacting system, which formulates Eq. (2) in terms of an effective single-particle potential:

$$\left[-\frac{\hbar^2}{2m}\nabla^2 + V_s(\mathbf{r})\right]\phi_i(\mathbf{r}) = \epsilon_i\phi_i(\mathbf{r}) \tag{3}$$

where ϕ_i are the orbitals that reproduce the density of the original many-body system ($n_s(\mathbf{r}) = \sum_{i=0}^{N}\phi_i(\mathbf{r})^2$). Under the K–S ansatz, the effective single-particle potential can be written as:

$$V_s(\mathbf{r}) = V(\mathbf{r}) + \int \frac{e^2 n_s(\mathbf{r}')}{\mathbf{r}-\mathbf{r}'}d^3\mathbf{r}' + V_{xc}[n_s(\mathbf{r})] \tag{4}$$

where n_s is the charge density, the second-term denotes the Hartree term describing the electron–electron Coulomb repulsion, and the final term is the exchange-correlation potential that includes all the many-particle interactions. In practice, the exact functional for exchange and correlation (and, in consequence, the exact V_{xc}) is not known and the development of approximate functionals that permit the calculation of certain physical quantities accurately is the focus of much research. One of the earliest density functionals, which is still in widespread use today, is the local density approximation, or LDA, where the functional depends only on the density at the coordinate where the functional is evaluated. A slightly more advanced approximation incorporates the gradient of the density as well following the generalized gradient approximation, or GGA [13, 14]. Both GGA and LDA functionals are fitted on the free electron gas for which the exact exchange and correlation functional is known.

Total energies

One of the main "outputs" from solving the K–S equations for a material is its ground-state energy. This fundamental property of a material already provides immensely useful information for materials scientists. For example, the ground-state energy can be used to identify the most stable polymorph of a particular chemical composition, to calculate reaction, binding, and defect energies and to assess phase stability.

In addition, by calculating the change in energy for small displacements about the equilibrium ion positions, we can also compute the phonon spectra for a material. Phonon modes are of importance, for example, in detecting ferroelectricity or incorporating finite-temperature vibration effects into phase stability analysis. Total energy calculations can also be used to estimate reaction and diffusion barriers by calculating energy changes along a reaction or diffusion pathway (e.g., by using the nudged elastic band (NEB) method [15, 16]). Reaction barriers are important in catalysis design, while diffusion pathways are important when studying ionic or polaronic transport.

A significant problem with semi-local functionals such as the LDA and GGA is that they contain a spurious electron self-interaction (SI) energy. This spurious SI energy leads to considerable errors in reactions energies for which electrons are transferred between significantly different environments, such as a metal and a transition metal oxide. Intense efforts have been focused at alleviating the self-interaction issue. One popular approach, which does not increase the computational burden compared to GGA or LDA, is to use a so-called Hubbard U parameter that will cancel part of the SI energy on the most problematic orbitals such as localized d- or f-orbitals [17, 18]. The DFT+U method requires the determination of an adequate U parameter that can be computed through self-consistent linear response theory [19] or by a fit to the experimental formation energies [20, 21]. Alternatively to DFT+U, researchers have been incorporating a fraction of exact Hartree–Fock exchange through hybrid functionals as in the Heyd–Scuseria–Ernzerhof (HSE) functional especially suited for solid-state applications [22–25]. These hybrid approaches are, however, more computationally expensive than DFT+U.

Electronic structure properties

Another property of significant interest is a material's electronic structure. Solving the Kohn–Sham equation provides directly the charge density of a material which can give insight into charge localization and the nature of bonding or, in the case of spin-polarized systems, provide the magnetic moments on different atoms.

In addition, from the Kohn–Sham orbitals, band structures can be obtained which are of interest in applications as varied as photovoltaics, thermoelectrics, or electronics. However, the accurate prediction of band structures using DFT is currently a major challenge. For instance, it is well-

known that semi-local functionals such as LDA and GGA systematically underestimate the energy gaps between occupied and unoccupied states in solids by 30–100 % [26]. This underestimation has been attributed to the inherent lack of derivative discontinuity [27] and delocalization error [28].

Several approaches have been developed to address the limitations of semi-local functionals with respect to electronic structure properties. For example, the hybrid HSE functional, which incorporates a fraction of exact Hartree–Fock exchange, has been demonstrated to lead to much more accurate band gaps [24, 29]. Excited-state methods such as GW [30, 31] and time-dependent DFT [32] can also provide more reliable predictions of electronic structure, and optical properties. However, most of these methods are significantly more computationally expensive (at least an order of magnitude or more) than LDA or GGA, and current efforts are directed toward the development of cheaper (but often slightly less accurate) methods such as the Tran–Blaha potential [33], the GLLB-SC model potential [34, 35], or the Δ-sol method [29].

Compound and crystal structure prediction

As presented in the previous section, modern first-principles theory provides researchers with many powerful tools to compute different properties of materials. This opens up the possibility of computing the properties of interest of a targeted material even before any experimental measurement has been made. One can for instance easily think that in search of a good photovoltaic material, computing the band gap of several candidates would help to identify compounds able to absorb light at a an adequate wavelength. Often, researchers search for promising materials by computing properties on previously known compounds (or small modifications of them) obtained from the literature or from a crystal-structure database. However, there are potentially many undiscovered inorganic compounds, some of which might have excellent properties for specific applications, motivating the computational search of novel compounds and their crystal structure.

In 1988, the poor status of this crystal-structure prediction problem made *Nature*'s editor John Maddox call it "one of the continuing scandals in the physical sciences" [36]. Since then, the computational prediction of new compounds before synthesis has improved substantially due to advances in ab initio techniques, and as we will briefly overview in the coming paragraphs, also in crystal-structure prediction algorithms [37–39].

The first necessary ingredient for the prediction of compounds is the ability to evaluate computationally their thermodynamical equilibrium phase stability. Simply put, one needs to know if a proposed novel compound is stable versus all competing phases. This can be performed using total energies computed with DFT, with the careful use of adequate functionals and methods (e.g., DFT+U) [40–42]. While advanced DFT techniques can be accurate enough to model stability successfully [43], a large part of the challenge lies in the second ingredient for compound predictions, which is the efficient selection of compound candidates to test for stability. This selection is typically performed following one of two approaches: optimization or data mining-based.

Optimization approaches

Finding the most stable crystal structure (at a given composition) can be mapped to the mathematical problem of finding the values of the structural degrees of freedom (i.e., lattice parameters and atomic positions) minimizing the (free) energy. The search for a global minimum on the energy landscape is, however, far from simple as the energy function (or landscape) is very large, complex and presents many local minima (see Fig. 1) [44].

One popular way of simplifying this problem has been to reduce the number of degrees of freedom by working on a fixed-crystal lattice, only allowing different decorations of an underlying crystalline framework. For instance, we can study any ordering on a face-centered cubic lattice at a composition AB and possibly find a rock-salt ground-state. This approach is usually coupled with the use of a simplified hamiltonian fitted on a limited set of computations performed on selected orderings through the cluster expansion technique [45, 46]. Identifying new phases on a

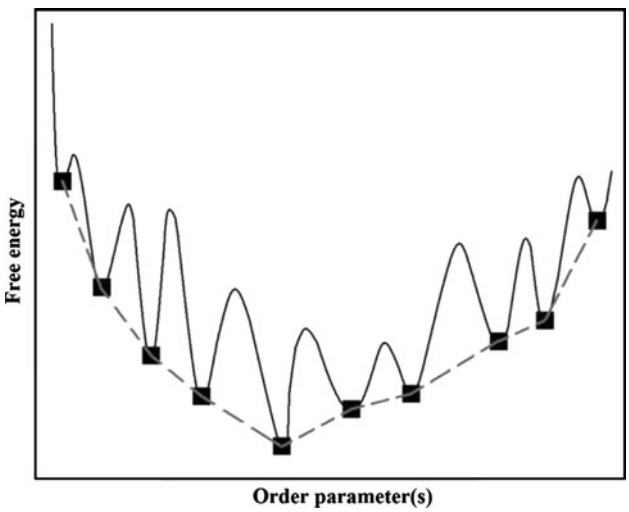

Fig. 1 Conceptual depiction of an energy landscape [44]. The order parameter(s) represent the degrees of freedom of the crystal. The energy landscape has many local minima (*black squares*) and is very rugged. Reprinted with permission from [44]. Copyright 2009, American Institute of Physics

fixed-lattice has been especially useful in alloy theory [47–49], but close-packed oxides have also been studied through cluster expansion [50].

However, when the underlying lattice is not known, researchers must rely on advanced optimization techniques such as simulated annealing or genetic algorithms to explore the rugged energy landscape. Simulated annealing (and the related basin hoping) [51, 52] rely on applying perturbations to a starting configuration. These perturbations are accepted or not depending on the change in energy, offering a way to efficiently scan the energy landscape in search of a global minimum. Genetic algorithms on the other hand are inspired by the biological process of evolution and the idea of survival of the fittest [53–57].

Optimization methods have been used to study many different chemistries, often with empirical potentials. However, a growing number of studies are now being performed using first-principles computations (e.g., the Na-N [58], W-N [59], and Fe-B [60] chemical systems). New phases proposed by optimization approaches and recently confirmed experimentally include a new high-pressure phase of Boron (although using the experimentally determined cell parameters as input) [59], a new high-pressure phase of $CaCO_3$ [55, 61], or a new metastable polymorph of LiBr [62, 63]. The optimization approach to structure prediction is very appealing but suffers from very large requirements in terms of computational budget, especially when multicomponent systems are explored.

Data-mining approaches

As an alternative to optimization-based techniques, researchers have been developing data mining or machine learning techniques that learn from previous computations or experiments and make informed guesses about likely crystal structure candidates [64].

The pioneering work from Curturalo et al. [65] consisted in using linear regression analysis to use information from previous computations to predict the energy of not yet computed compounds. Subsequently, Fischer et al. [66], proposed to use data from an experimental structure database to extract the chemical rules of structural stability using correlation between crystal structures at different compositions. Very recently, a new technique more efficient in data sparse regions (e.g., quaternary compounds) and based on the data mining of ionic substitution has been proposed by Hautier et al. [67]. All of these data mined techniques are always used in combination with DFT which finally assess if the short-list of candidates proposed through data mining techniques are indeed stable.

While less exhaustive than optimization techniques, knowledge-driven methods have much lower computational requirements which make them more suitable for large-scale high-throughput searches of new materials. These techniques have already been used to perform searches of new materials and proposed for instance new borides [68, 69], rhodium alloys [70], or ternary oxides [71, 72].

Using data-mined techniques, it was recently predicted that $SnTiO_3$ (at the time unsynthesised) would be stable in a distorted ilmenite structure [71]. A few months later, $SnTiO_3$ was synthesised and experimental measurements confirmed the predicted ilmenite structure [73]. Interestingly, $SnTiO_3$ in the perovskite structure had been presented in several computational works to be of interest as a lead-free piezoelectric [74, 75] but the ilmenite structure is unfortunately not piezoelectric. This example is not only a clear success for compound prediction but also illustrates the importance of considering the phase stability of the specific crystal structure when computationally designing materials. More examples of data-mined compound predictions confirmed experimentally will be given in "Lithium-ion batteries" section covering Li-ion battery design.

The use of compound prediction techniques for the discovery of new materials of technological interest has still been limited but we are convinced that the recent developments in compound prediction algorithms, the availability of new codes (e.g., genetic algorithm USPEX and MAISE codes [76, 77]) and web interfaces (e.g., data-mining structure prediction [78]), as well as the crystal-structure prediction expertise building in fundamental fields (e.g., high-pressure phases in geophysics) will lead to many compound predictions for technological applications in the near future.

Case studies

After this brief overview of the computational methods available to materials designers, we will now turn to the core of our review by presenting and discussing examples in which computational tools were used to predict the behavior of materials that were confirmed experimentally subsequently. The section will be divided by applications, starting with energy applications, going through magnetic, multiferroic and electronic materials, and finishing with catalysis.

Energy applications

The reasons to switch from an energy economy primarily powered by fossil fuels to renewable resources include reduced pollution, more stable pricing, and improved energy independence of nations. A critical challenge present for almost all renewable energy technologies is to find low-cost, earth-abundant materials that also meet high performance requirements [79, 80]. A selection of such challenges

include: materials to efficiently capture and convert sunlight to energy; stiff, failure resistant alloys for wind turbines; corrosion-resistant alloys for nuclear power plant vessels; high figure-of-merit thermoelectric materials; catalysts for fuel cells; materials for hydrogen storage; and low-cost and high performance battery components. Materials advances in these areas are potentially game-changing. For example, it has been estimated that two-thirds of gasoline use in the United States could be eliminated if vehicles were powered by electricity for 60 km (about 37 miles), demonstrating the need for better energy storage materials [81].

In this section, we examine ab initio predictions of materials relevant to energy storage, Li-ion batteries and hydrogen, and energy production from thermoelectric materials.

Lithium-ion batteries

The Li-ion battery is the most common type of energy storage in consumer electronics and it is strongly considered for emerging applications. These new areas of application include the transportation sector (electric vehicles) and load leveling of the power grid (which is especially important for intermittent power sources such as wind and solar). For electric vehicles, the Li-ion battery will likely be the dominant energy storage technology for the foreseeable future. While the future is still uncertain, a report from IHS predicts that global lithium-ion battery revenue will grow from $11.8 billion in 2010 to $53.7 billion in 2020, and that electric cars will become the largest single market for Li-ion batteries within the next 5 years [82].

A Li-ion battery contains two electrodes, the anode and cathode, which are Li-insertion materials. The anode is most commonly graphitic carbon, whereas the cathode might be one of several chemistries such as Mn- and Ni-doped $LiCoO_2$, spinel $LiMn_2O_4$, or olivine $LiFePO_4$. The anode and the cathode are separated by an electrolyte that permits the flow of Li^+ ions but not electrons. The electrons flow through an external circuit to perform work.

When a Li-ion battery is discharged, Li-ions move from the anode to the cathode. Taking the case of graphitic carbon for the anode and $LiFePO_4$ for the cathode, the anode reaction upon discharge is:

$$LiC_6 \longrightarrow Li^+ + e^- + C_6 \quad (5)$$

and the cathode reaction is:

$$Li^+ + e^- + FePO_4 \longrightarrow LiFePO_4 \quad (6)$$

The reverse reactions occur upon charge. Neglecting the (significant) weight and volume of the inactive components, the energy stored by the battery is the product of two properties: its capacity and its operating voltage. The electrode capacity of the battery, measured in mAh/g or mAh/cc, is the amount of charge transferred per unit weight or unit volume of the electrodes. In the example above, one electron of charge is transferred per formula unit of LiC_6 and $LiFePO_4$. One way to improve the energy density of Li-ion batteries is to improve capacity either by reducing the mass or volume of the electrode materials or by transferring multiple electrons per formula unit. A second method is to increase voltage, which is the energy stored per unit of charge; however, voltages above about 4.5 V can be problematic as they often lead to side reactions with the electrolyte. The voltage can be easily obtained using DFT from two total energy computations (one for the charged and one for the discharged state) [83].

In addition to voltage and capacity, other critical properties for Li-ion batteries, including rate capability (through electronic [84] and ionic [85] limitations) and safety [86], have been successfully modeled by first-principles computations [87–89]. In this section, we focus on the cathode due its large contribution to the overall cost, weight, and volume of the cell and the significant amount of theoretical work in this area.

Voltage modification in $LiCoO_2$ through Al-doping As mentioned in the previous section, one method to increase the energy density of the cathode is to increase its voltage. A 1998 study by Ceder et al. [90] introduced a new idea to increase the voltage of cathode materials: by reducing the amount of transition metal in the composition, a greater amount of charge would be transferred to the anion, leading to a lower electrostatic energy and higher voltage. Specifically, they hypothesized that replacing some of the transition metal M in layered $LiMO_2$ cathodes with inactive Al would lead to higher voltages.

Although previous experimental studies had shown no effect of Al substitution in layered $LiMO_2$ systems, Ceder et al. systematically computed both the voltages and Al mixing energies of $LiMO_2$ systems. Crucially, they found that of all the $LiMO_2$ systems, only $LiCoO_2$ would favorably incorporate Al; transition metals other than Co would phase-separate upon addition of Al, explaining why no voltage change had been observed in previous investigations of Al-doping [90]. In addition, they predicted that the voltage increase would be significant: about 0.5 V per 33 % Al-doping [90].

Based on the computations, Ceder et al. [90] targeted $Li(Co,Al)O_2$ solid solutions. The results indeed demonstrated significant voltage increases of about 0.15 and 0.3 V for 25 and 50 % Al-doping, respectively (Fig. 2). Although the measured voltage increase was about half of what was computationally predicted, the computational work unequivocally produced the right qualitative results and guided the experiments to $LiCoO_2$ as the suitable test system for Al-doping.

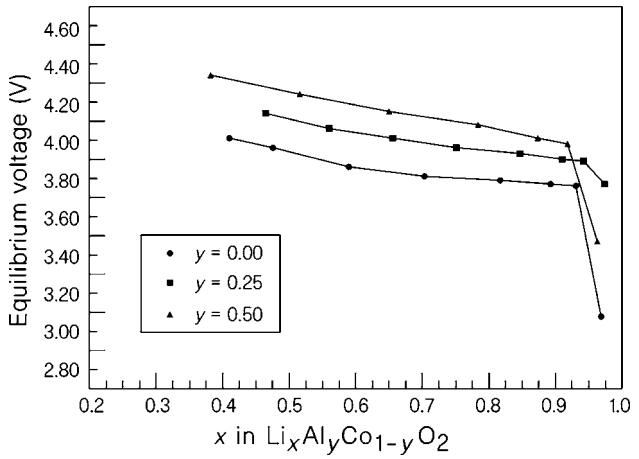

Fig. 2 Measured voltage of $Li_xAl_yCo_{1-y}O_2$ cathodes as a function of lithium content for three different levels of Al-doping [90]. The experimental data confirms the theoretical work of the same group predicting that Al-doping would result in higher voltages. Reprinted by permission from MacMillan Publishers Ltd: Nature [98], copyright 1998

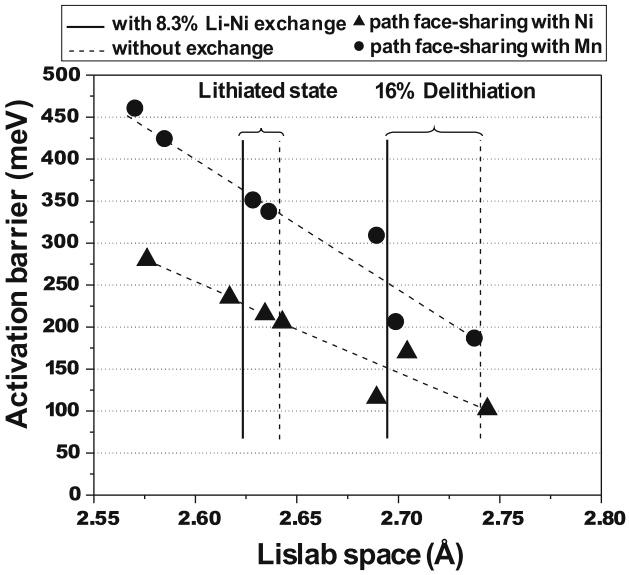

Fig. 3 The predicted effect of Li slab spacing on activation barriers for Li migration in layered $Li(Mn_{0.5}Ni_{0.5})O_2$ [91]. The data indicates that larger slab spacings will lead to lower Li-migration barriers, and subsequently higher rate capability of $Li(Mn_{0.5}Ni_{0.5})O_2$ electrodes. Experimental work by the same team on ion-exchanged versus conventional $Li(Mn_{0.5}Ni_{0.5})O_2$ samples confirmed the prediction. From [91], reprinted with permission from AAAS

High-rate $LiMn_{0.5}Ni_{0.5}O_2$ Apart from the energy density (driven by capacity and voltage), many applications, including transportation, require the ability to charge and discharge the battery at a high rate. DFT investigations of rate capability generally focus on activation barriers for Li motion in the bulk, which are used to crudely approximate the Li diffusion coefficient. Activation barriers for Li motion can be evaluated using NEB calculations [15, 16]. Thus, calculations can in principle be used to design new materials with good potential rate capability. An example of such a study was conducted by Kang et al. [91] on the optimization of $LiMn_{0.5}Ni_{0.5}O_2$.

$LiMn_{0.5}Ni_{0.5}O_2$ is a desirable cathode material because octahedral Mn^{4+} ions stabilize the layered structure during cycling, whereas $Ni^{2+/4+}$ provides an electron acceptor at a desirable voltage. However, $LiMn_{0.5}Ni_{0.5}O_2$ synthesised by solid-state reaction suffers from relatively poor rate capability. Kang et al. [91] investigated computationally the Li diffusion mechanisms in this system, finding that the activation barrier of Li was extremely sensitive to the spacing between oxygen layers. The computational results indicated that even small oxygen layer spacing reductions of 0.02 Å led to large 20–30 meV reductions in the activation energy (Fig. 3).

To synthesize $LiMn_{0.5}Ni_{0.5}O_2$ with larger layer spacings, Kang et al. [91] noted that conventional synthesis leads to disorder between Li and Ni. Further calculations demonstrated that this disorder reduces layer spacing, and thereby inhibits fast Li diffusion [91]. To achieve high rates, Kang et al. synthesised ordered $LiMn_{0.5}Ni_{0.5}O_2$ by ion exchanging Li into ordered $NaMn_{0.5}Ni_{0.5}O_2$. The ordered $LiMn_{0.5}Ni_{0.5}O_2$ significantly outperforms conventional $LiMn_{0.5}Ni_{0.5}O_2$ at high-rates, in agreement with theoretical predictions [91].

Thus, the design principle of achieving higher rate capability by tuning layer spacing was confirmed experimentally. Despite the successful demonstration of a novel high-rate cathode material guided by DFT computation, ordered $LiMn_{0.5}Ni_{0.5}O_2$ presently suffers from poor capacity retention upon repeated cycling, and studies to better understand its behavior are in progress.

High-throughput studies $LiMnBO_3$, $Li_9V_3(P_2O_7)_3(PO_4)_2$, $Li_3MnPO_4CO_3$ Because many cathode properties can be predicted by using only total energy calculations, the search for new cathode materials can be semi-automated. In particular, potential cathode chemistries can be screened on voltage, volume change, stability upon Li removal/insertion, thermal safety, and, to some extent, Li diffusivity. Such a study was conducted by Ceder and co-workers, who screened tens of thousands of cathode materials, including both known compounds and yet-unknown compounds generated using data-mined compound prediction algorithms (Fig. 4). Here, we highlight novel cathode materials that were guided by this high-throughput search.

Monoclinic $LiMnBO_3$

Borates are an interesting class of materials for cathodes because they possess attractive voltages and fairly large

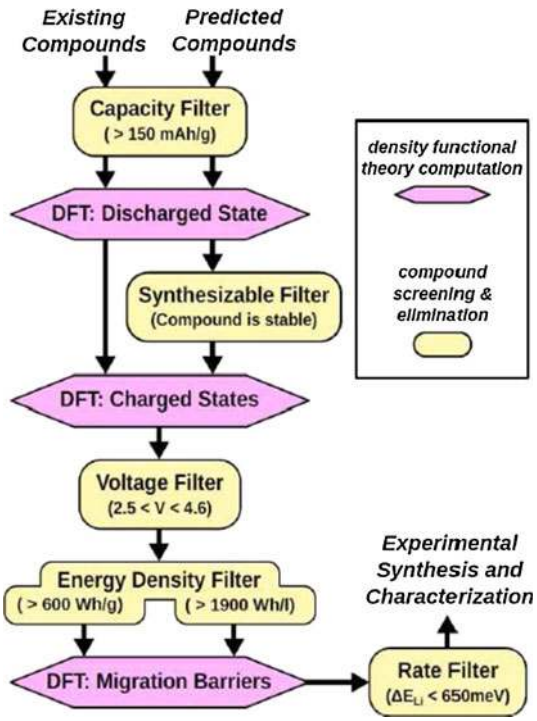

Fig. 4 Flow chart for high-throughput screening of battery cathode materials [92]. Similar to many screening workflows, the procedure is tiered so that relatively inexpensive calculations (total energy evaluations of the discharged and charged states) narrow down the candidates to a smaller list. The more computationally expensive migration barriers are calculated only for candidates passing the pre-screening

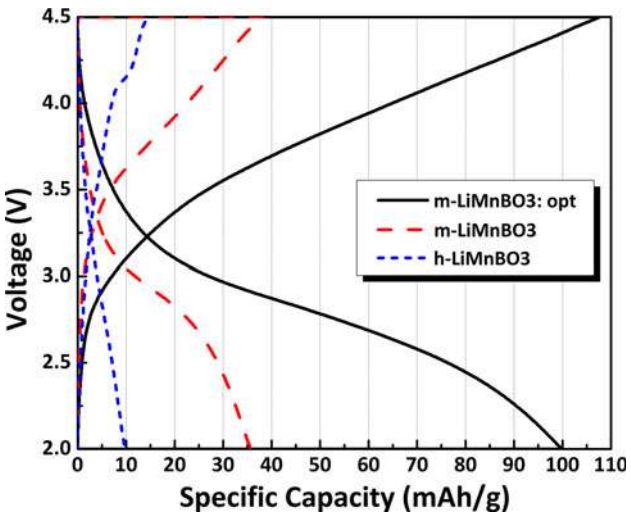

Fig. 5 Measured electrochemical performance under galvanostatic conditions for two different crystal structures of $LiMnBO_3$ at C/20 rate. Kim et al. [94] predicted that the untested monoclinic version might be more promising than the conventional hexagonal structure. The experimental data confirms the prediction: the hexagonal compound (h-$LiMnBO_3$) produces a capacity of only about 10 mAh/g whereas unoptimized monoclinic $LiMnBO_3$ (m-$LiMnBO_3$) displays a capacity that is at least three times greater. Further optimization with carbon coating and ball-milling results in a capacity of about 100 mAh/g for the monoclinic form (m-$LiMnBO_3$: opt). Reproduced with permission from [94]. Copyright 2011, The Electrochemical Society

capacities due to the high charge-to-weight ratio of the borate chemical group. $LiMnBO_3$ is a borate that crystallizes in both a low-temperature monoclinic and high-temperature hexagonal form. The hexagonal form had been investigated previously but had demonstrated very poor capacity in experiments [93]. However, the monoclinic form remained untested as a cathode.

High-throughput calculations over the known materials revealed that monoclinic $LiMnBO_3$ was a promising electrode material possessing several advantages over its hexagonal counterpart: a more stable delithiated state, a lower activation energy for Li migration, and a lower voltage that might be less susceptible to side reactions with the electrolyte [94]. These characteristics hinted that although hexagonal and monoclinic $LiMnBO_3$ have the same theoretical gravimetric capacity, the capacity of monoclinic $LiMnBO_3$ achievable in practice might exceed that of the hexagonal form.

Based on this data, monoclinic $LiMnBO_3$ was synthesised and tested as a cathode [94, 95]. As suggested by the calculations, the monoclinic form initially demonstrated about three times the gravimetric capacity of the hexagonal form (Fig. 5). In addition, monoclinic $LiMnBO_3$ displayed even greater capacity, about ten times that of its hexagonal counterpart, with some optimization of the ball-milling and carbon coating method (Fig. 5).

High-throughput computations helped reveal monoclinic $LiMnBO_3$ as a strong materials candidate that was somehow missed by experimental study alone. Thus, one of the great advantages of large-scale computational searches is their systematic and comprehensive nature.

$Li_9V_3(P_2O_7)_3(PO_4)_2$

In addition to the previously known $LiMnBO_3$ monoclinic phase, the high-throughput search coupled with a data-mined compound prediction algorithm [67] identified a previously unknown layered diphosphate–phosphate materials, $Li_9V_3(P_2O_7)_3(PO_4)_2$ as likely to be synthesizable and displaying attractive cathode properties (i.e., an attractive voltage, a theoretical energy density about 20 % higher than $LiFePO_4$, and fair safety).

Experimental reports of synthesis and promising electrochemical performance from $Li_9V_3(P_2O_7)_3(PO_4)_2$ came from two groups. The high-throughput team of Ceder et al. [96] reported on the synthesis and electrochemical properties of $Li_9V_3(P_2O_7)_3(PO_4)_2$ in a patent filing. However, $Li_9V_3(P_2O_7)_3(PO_4)_2$ was also synthesised and tested independently by Kuang et al. [97, 98]; their report was published after Ceder et al.'s patent filing, but prior to any computational results being published by Ceder and

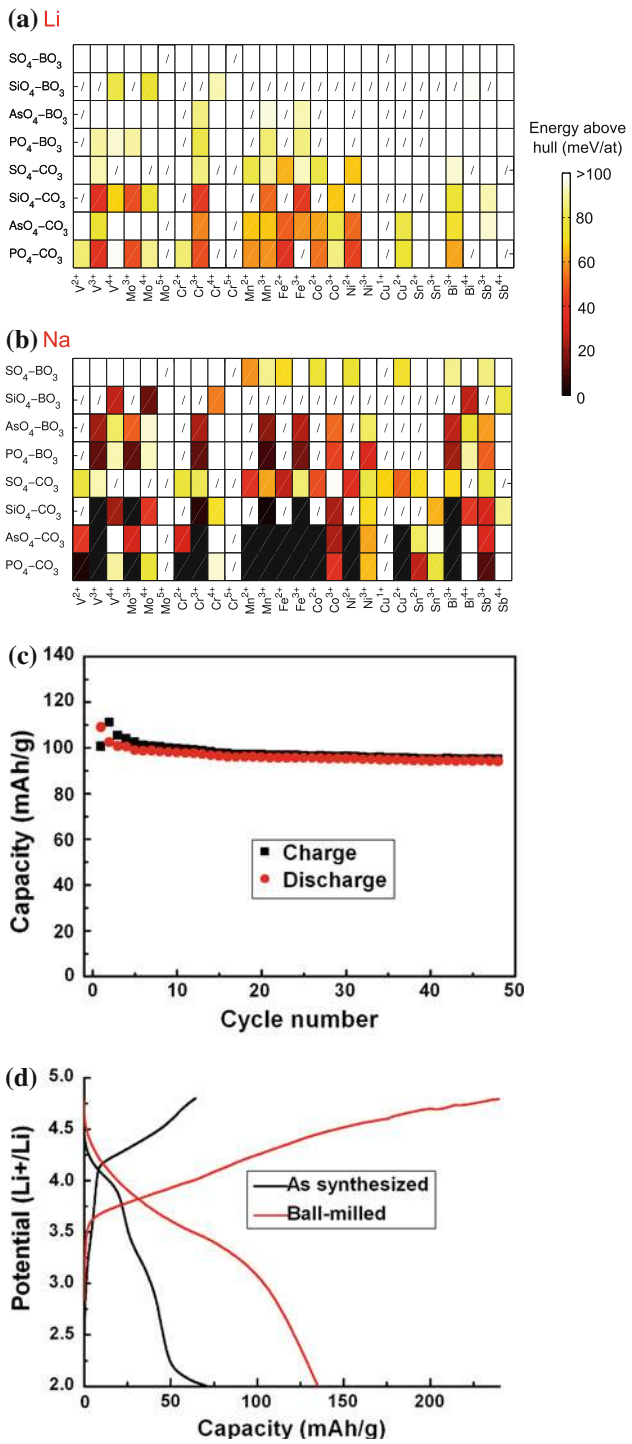

Fig. 6 **a** and **b** Computed stability for different combinations of active element and polyanion mixtures in the sidorenkite structure [100]. The energy above the hull is an indicator of instability: lower energies above the hull indicate a smaller driving force for decomposition (greater stability). The "/" indicate non-computed combinations. The computational study identified the CO_3–PO_4 mixtures to be the most stable and suggested that the compound might be synthesised by first forming the Na phase and performing a Na–Li ion-exchange. **c** Cycling data for $Li_3Fe(CO_3)(PO_4)$ at a C/5 rate, indicating the good cycling performances for the sidorenkite structure [92]. **d** The voltage versus capacity curve for the $Li_3Mn(CO_3)(PO_4)$ compound with residual sodium at a C/100 rate, after synthesis and with an additional ball-milling step [92]. Figure **a** and **b** from [100]. Reproduced by permission of the Royal Society of Chemistry (RSC)

coworkers. Kuang et al.'s discovery of $Li_9V_3(P_2O_7)_3(PO_4)_2$ therefore came independently of and around the same time as that of Ceder et al. Both groups have demonstrated $Li_9V_3(P_2O_7)_3(PO_4)_2$ to be one of only a few known materials capable of exchanging multiple electrons per transition metal (through the V^{3+} to V^{5+} redox couple). Although neither group has yet attained the full theoretical capacity (around 170 mAh/g), a reversible capacity of about 140 mAh/g was obtained by Kuang et al. [98]. Follow-up calculations by Jain et al. indicate that doping might be needed to further improve the experimentally realized capacity [99].

Although further experimental work is needed on this compound, it already represents a rare example in which an entirely new phase of technological interest in an uncommon crystal structure and stoichiometry was discovered computationally and subsequently made in the laboratory.

Sidorenkites: $Li_3Fe(CO_3)(PO_4)$, $Li_3Mn(CO_3)(PO_4)$

Cathode materials including polyanionic groups such as PO_4^{3-}, SiO_4^{4-}, or BO_3^{3-} are of great interest in the battery community but materials with a combination of those groups have been less explored. Similarly to $Li_9V_3(P_2O_7)_3(PO_4)_2$, the high-throughput battery screening project identified a completely new class of mixed polyanion compounds: the lithium metal carbonophosphates $Li_3M(CO_3)(PO_4)$ in the crystal structure of the rare mineral sidorenkite [100, 101]. These compounds are of interest for cathode materials due to their low volume change during delithiation (which is beneficial for cyclability) and a potential for high capacity due to the large lithium content (>200 mAh/g).

Of the potential $Li_3M(CO_3)(PO_4)$ compounds, the most interesting candidate was predicted to be $Li_3Mn(CO_3)(PO_4)$ which is computed to activate the Mn^{2+}/Mn^{4+} redox couples in an adequate voltage range (between 3 and 4.5 V) and has a large theoretical specific energy of about 800 Wh/kg (versus about 600 Wh/kg for the current polyanionic compound $LiFePO_4$). A comprehensive phase stability analysis on all $A_xM(YO_3)(XO_4)$ compounds in the sidorenkite structure (with A = Li or Na, M a redox active metal, Y = C or B, and X = P, Si, As, or S) indicated that the carbonophosphates were indeed the most stable chemistries but that all $Li_3M(CO_3)(PO_4)$ compounds are somewhat unstable and might be difficult to synthesize directly. On the other hand, many Na compounds are stable

according to computations, suggesting synthesis route was proposed in which Li-Na ion-exchange could be performed on the stable Na analog (Fig. 6a, b) [100].

Based on the theoretical study, Chen et al. subsequently synthesised the $Li_3M(CO_3)(PO_4)$ (M = Mn, Fe, Co, Ni) materials using hydrothermal synthesis of the Na phase followed by Na–Li ion-exchange [92]. Experiments on the iron version, $Li_3Fe(CO_3)(PO_4)$, demonstrated that only half of the expected capacity could be extracted, in line with theoretical predictions that the second voltage step of $Li_3Fe(CO_3)(PO_4)$ occurs at high voltages that would be hard to access with conventional electrolytes. However, $Li_3Fe(CO_3)(PO_4)$ demonstrated very good cyclability, indicating that the sidorenkite structure can indeed sustain multiple Li-intercalation cycles (see Fig. 6c). The more promising Mn analog thus far has not achieved the full theoretical capacity, which might result from residual Na after the ion-exchange, but has shown activity in the voltage range predicted computationally (Fig. 6d) [92].

This example illustrates how entirely new chemistries of technological interest can be identified through computations. Indeed, carbonophosphates are rare minerals that had no known technological application before their computational identification. It also shows that computations can effectively drive synthesis by providing likely synthesis routes (here a Na–Li ion-exchange) based on stability analysis.

Hydrogen storage

Hydrogen is a potential medium for storing and transporting energy. Hydrogen can be cleanly generated, either through electrolyzers or through water-splitting solar cells, and its energy content can be released pollution-free through fuel cells. There are many interesting materials problems in obtaining efficient photocatalysts to carry out water-splitting for hydrogen generation as well in finding catalysts for use in hydrogen fuel cells, both of which will drive down the cost of using hydrogen as an energy carrier (see "Catalysts for production and activation of H_2" section). However, we focus in this section on the problem of densely and reversibly storing hydrogen as a fuel.

The most direct forms for hydrogen storage are as a compressed gas, which suffers from low energy density, or as a liquid, which sacrifices 30–40 % of the energy stored during the liquefaction process [102]. Therefore, much research is being directed toward discovering solid metal hydrides that have a high percentage of hydrogen by weight or volume, have favorable thermodynamics for hydrogen release/absorption at about 100 °C, and can absorb and release hydrogen at high rates. At present, most DFT research has concentrated on the first two questions by clarifying the reaction pathways by which hydrogen is released in a material (thus determining percent of usable hydrogen) and by computing the thermodynamic (free) energy of the reactions. An overview of first-principles approaches to addressing hydrogen storage can be found in several excellent reviews [103, 104].

$LiNH_2$–MgH_2 (1:1) as a hydrogen storage material

Trends in thermodynamic hydrogenation and dehydrogenation energies can be reliably obtained using zero *K* total energy calculations. The straightforward nature of these calculations make it possible to conduct large-scale computational studies that test the thermodynamic feasibility of hundreds of potential hydrogen storage materials. One such study was conducted by Alapati et al. [105] on over 100 dehydrogenation reactions. These reactions generally involved one or multiple ternary metal hydrides reacting to form hydrogen gas and non-hydrogenated binaries such as metal borides, silicides, or nitrides.

Alapati et al. [105] reasoned that, given typical entropies of hydride reactions, the reaction enthalpy of dehydrogenation should target the range of about 30–60 kJ/mol—H_2. Neglecting kinetic considerations, a reaction enthalpy in this range would allow for both uptake and release of hydrogen near the target temperature range between 50 and 150 °C. Using this simple metric, Alapati et al. computed the energies of over 100 dehydrogenation reactions involving 49 unique compounds taken from experimental databases (see Fig. 7).

From the computed reactions, the researchers determined five new reactions that were not previously reported in

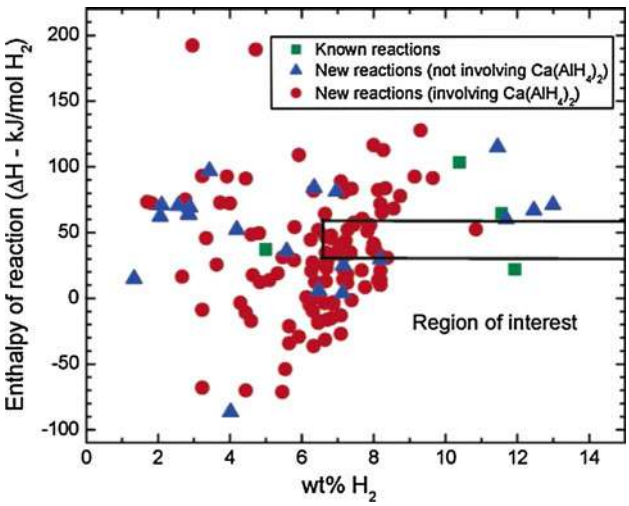

Fig. 7 Reaction enthalpies and capacities for 129 hydrogen storage reactions predicted by Alapati et al. [105]. The region of interest indicates reactions that possess both a high-hydrogen storage potential and a favorable reaction enthalpy. The data suggests several new potential hydrogen storage reactions, including $LiNH_2$:MgH_2 mixed in a (1:1) ratio which was subsequently confirmed experimentally [106]. Reprinted with permission from [105]. Copyright 2006, American Chemical Society

the experimental literature [105]. Thus, the computational study narrowed the initial search space by a factor of over twenty and reduced the candidate reactions to a number that could reasonably be tested by experiments. One of the five reactions suggested was a simple 1:1 reaction of $LiNH_2$ with MgH_2 that theoretically releases 8.19 wt% H:

$$LiNH_2 + MgH_2 \longrightarrow LiMgN + 2H_2 \quad (7)$$

The enthalpy of this reaction was computed to be about 30 kJ/mol—H_2 [105]. It is worth noting that mixtures of $LiNH_2$ and MgH_2 were previously tested for hydrogen storage [107], but in a 2:1 ratio rather than the 1:1 ratio proposed computationally. This 2:1 ratio has a lower theoretical capacity of about 5.4 wt% H, and experiments by Luo [107] on this ratio had yielded about 4.5 wt% H with a decomposition energy of 34 kJ/mol.

Experimental confirmation of Alapati et al.'s prediction came shortly afterward from Lu et al. [106], who obtained a capacity of 8.1 wt% of H from $LiNH_2$:MgH_2 (1:1). The enthalpy of reaction was measured to be 33.5 kJ/mol—H_2, close to the 30 kJ/mol theoretical prediction [105]. However, Lu et al. [106] found that activating the reverse reaction required a catalyst, and likely did not yield back the starting products.

In contrast to these experimental results, studies by both Osborn et al. [108] and Liu et al. [109] found that $LiNH_2$:MgH_2 (1:1) underwent different reaction pathways than suggested by the computations, and correspondingly found different storage capacities. The discrepancy between these measurements was addressed by Lu et al. [110], who suggested that low energy ball-milling would yield the reversible 8.1 wt% H capacity that they originally reported [106], whereas high-energy ball-milling would yield other reactions. The choice of ball-milling method was therefore crucial to the final performance of the material.

The case of $LiNH_2$:MgH_2 (1:1) illustrates the power of relatively straightforward theory, automated over many compounds, to provide guidance into further experiments. Although the $LiNH_2$:MgH_2 system was already studied experimentally, the comprehensive nature of large-scale calculation revealed a new and promising mixing ratio that had until then eluded experimental consideration. As it is often the case, however, the computational discovery had to be followed up by optimization of the factors not taken into account in the modeling such as the sample preparation (i.e., low energy vs high-energy ball-milling) and the kinetics of the system.

Thermoelectrics

Thermoelectrics are materials that generate voltage from a temperature differential (the Seebeck effect). They can also be operated in reverse to drive a temperature difference, most often for cooling (the Peltier effect). For power generation, well-established applications have primarily been for space missions, whereas emerging applications include co-generation of power with solar cells, waste heat recovery from trucks, small and self-powered electronics, and large-scale waste heat recovery from power plants [111]. Thermoelectric cooling has found many niche consumer applications, such cooling of beverages, vehicle seats, and microprocessors.

The primary measure of performance for a thermoelectric material is its figure-of-merit ZT which is defined as:

$$ZT \equiv \frac{\alpha^2 \sigma T}{\kappa} \quad (8)$$

where T represents temperature, σ represents electronic conductivity, and κ represents thermal conductivity. The thermopower α (often called the Seebeck coefficient) is the voltage produced by a given temperature difference.

The figure-of-merit ZT, along with the ratio between the temperature of the hot and cold sides, determines the percentage of the Carnot efficiency a thermoelectric can attain. Researchers in the field generally seek materials with ZT >1 and ideally in the range of 2–3. A material with a ZT of 2–3 corresponds to an overall efficiency of about 25–30 % if the hot side is kept at 500 °C with the cold side at room temperature. While even greater ZT would be beneficial, there are diminishing returns with increasing ZT.

To produce a figure-of-merit >1, the thermopower α must be greater than about $150 \frac{\mu V}{K}$ (assuming fairly optimistic values for the other parameters) [112]. High thermopower is a necessary but insufficient condition for good performance. The other necessary condition is to have a high ratio between electronic and thermal conductivities, $\frac{\sigma}{\kappa}$ (Eq. 8). The thermal conductivity is generally expressed as separate electronic and lattice contributions, $\kappa = \kappa_e + \kappa_l$. Achieving a high ratio between the electronic contributions σ and κ_e is difficult because these quantities tend to be proportional to one another (for example, through the Wiedemann–Franz law in metals). Much research therefore focuses on minimizing the phonon contributions to the thermal conductivity, κ_l. This idea is succinctly summarized through the acronym PGEC (phonon glass and electron crystal), and realized through both nanostructured materials and bulk materials with "rattler" ions inside voids such as skutterudites and clathrates [113]. While a few design principles are available to achieve PGEC, it remains difficult to find materials with high ZT. Today's commercial thermoelectrics are generally bulk materials such as alloys of Bi_2Te_3, PbTe, and SiGe.

LiZnSb as a new thermoelectric A direct approach to predicting the thermoelectric figure-of-merit would involve calculating the thermopower α along with the electronic

conductivity σ and the thermal conductivities κ_e and κ_l (Eq. 8). However, it is challenging with present methods to compute all of these properties accurately even for a single material, let alone a diverse set of materials. Madsen simplified the problem by focusing on Sb-based alloys, using the Wiedemann–Franz relation to remove κ_e as a free variable, and setting κ_l to a reasonable constant [114]. The expression for figure-of-merit is thus simplified to:

$$ZT = \frac{\alpha^2}{L_0 + \frac{\kappa_l}{\sigma T}} \tag{9}$$

where L_0 is the Lorentz number and κ_l is set to a constant. Equation (9) leaves only the (still challenging!) problem of computing the thermopower α and electronic conductivity σ for a library of Sb compounds. These latter quantities were computed using a rigid band approach based on the Boltzmann equation along with an approximation for the electron relaxation time based on common Sb alloys. Under this approximation, the only computations needed to estimate the figure-of-merit were the band structures of the interesting Sb-based compounds.

As a search space, Madsen pre-screened 1670 Sb-based compounds from the Inorganic Crystal Structure Database (ICSD) [115, 116] to a list of 570 compounds based on chemical arguments as well as to avoid limitations of DFT in predicting properties of lanthanides and disordered compounds. One validation of the approach was that it found back chemical classes already known to be interesting such as the skutterudites. In addition, the search predicted that a known but untested compound, LiZnSb, could produce a high figure-of-merit between 1.35 and 2.36 at 600 K. Crucially, the results indicated that n- and p-types LiZnSb would behave very differently, with only n-type LiZnSb producing a high figure-of-merit.

The challenge to synthesize n-type LiZnSb was undertaken by Toberer et al. [117], who were able to synthesize LiZnSb but could only form the p-type material. Toberer et al. confirmed that Madsen's predicted thermopower of p-type LiZnSb at 500 K matched the experimental data to within a few percent (Fig. 8). The good match between computation and experiment on p-type LiZnSb lend credibility that n-type LiZnSb, if synthesizable, could yield the very high-predicted figure-of-merits. However, dopability was not addressed in Madsen's study [114], and it is possible that n-type LiZnSb would be extremely difficult to synthesize. The study has therefore demonstrated that its search strategy can pick out materials known to be interesting from a larger list and successfully predicted the thermoelectric properties of p-type LiZnSb prior to experimental measurements. In the future, an ab initio indicator of dopability through defect computations [118, 119] might improve the chances to find a viable new thermoelectric.

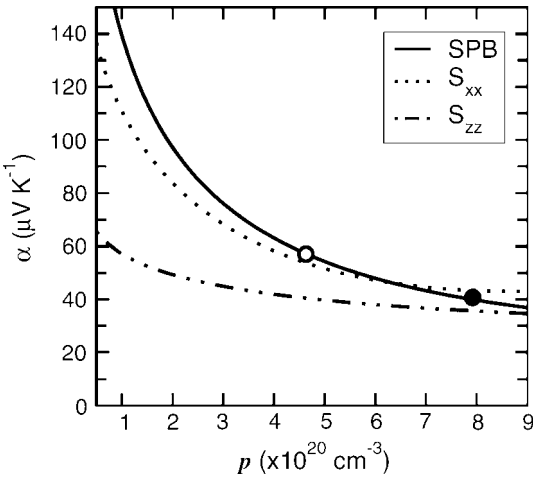

Fig. 8 Thermopower α versus doping level for p-type LiZnSb. The *circles* represent experimental data measured by Toberer et al. [117] at 500 K, and the *solid line* represents a fit to the experiment using a single-parabolic band model. The thermopower predicted by Madsen et. al using first-principles calculations is shown as dotted and dashed-dotted lines [114]. The agreement between prediction and experiment indicates that it might be possible to screen for materials possessing a high thermopower through computation. Reprinted with permission from [117]. Copyright 2009, American Institute of Physics

High thermopower in $FeSb_2$ A niche application for thermoelectrics is cryogenic cooling. An interesting class of compounds for this application is Kondo insulators. Kondo insulators are metallic at room temperature because the Fermi energy lies within the conduction band. However, at low temperatures, a metal-to-insulator transition occurs because the conduction band hybridizes with localized *d*- or *f*-states near the Fermi energy. The hybridization opens up a small gap leading to insulating behavior. In the vicinity of this transition temperature, there are large variations in the density of states close to the Fermi energy, leading to a high thermopower α.

It would be difficult to quantitatively predict Kondo insulators from DFT calculations because the Kondo effect depends on strong correlations, which are difficult for present-day DFT exchange-correlation functionals to quantitatively reproduce. Instead, Madsen et al. relied only on qualitative correlations in the calculated density of states (DOS) between $FeSb_2$, at that point unknown to be a Kondo insulator, and FeSi, a known Kondo insulator, to suggest that $FeSb_2$ might display a high thermopower due to the Kondo effect [120] (it should be noted that around the same time, the experimental work of Petrovic et al. similarly suggested $FeSb_2$ might be described as a Kondo insulator [121]). The similar DOS of FeSi and $FeSb_2$ was an unintuitive result because $FeSb_2$ and FeSi crystallize in different structures (marcansite versus a distorted rocksalt, respectively). The common fingerprint in both compounds was a high and steep DOS near the Fermi energy.

Based on the theoretical observation, Bentien et al. measured the low-temperature thermopower of $FeSb_2$, finding a peak at $-500\ \frac{\mu V}{K}$ at 25 K [122]. This high value was later surpassed by the same authors and Steglich, who measured a colossal thermopower of about $-45000\ \frac{\mu V}{K}$ at 10 K and a record-setting power factor $(\frac{\alpha^2}{\rho})$ of about $2300\ \frac{\mu W}{K^2}$ [123]. Unfortunately, despite the high thermopower, the actual figure-of-merit of $FeSb_2$ was measured to be very poor (0.005 at 12 K) due to a high-lattice thermal conductivity [123]. However, it is nonetheless interesting that even qualitative observations of DFT band structure calculations have the potential to guide record-breaking experimental measurements.

Electronic, magnetic, and ferroelectric materials

Materials with specific magnetic, ferroelectric, or electronic properties are essential in many applications such as sensors, integrated circuits, and information storage. Many of the properties of interest in these fields (e.g., band structures or magnetic moments) can be accessed directly through ab initio techniques, leading to several examples of computationally driven materials design.

Magnetic materials

Most of the current non-volatile information storage devices (e.g., hard disks) are based on magnetism and depend on ferromagnets (i.e., materials in which an applied magnetic field can induce a permanent magnetization). Simply put, binary information is stored by inducing or removing permanent magnetization in a ferromagnetic film through the application of a magnetic field [124, 125].

Magnetic ordering in multicomponent borides and nitrides For magnetic storage applications, it is important to be able to predict the exact nature of spin ordering in an inorganic compound: ferromagnetic (FM) with spins pointing in the same direction or anti-ferromagnetic (AFM) with spins pointing in opposite directions.

Dronskowski et al. [126] showed in a series of papers that the magnetic ordering of borides and nitrides could be predicted through DFT computations, enabling a chemical tuning of their magnetic behavior. Focusing on the series of $A_2MRh_5B_2$ compounds in the $Ti_3Co_5B_2$ crystal structure, they demonstrated that DFT computations could predict whether the magnetic ordering of a material would be AFM or FM. Starting with a known AFM compound, $Mg_2MnRh_5B_2$, they computed that combined substitutions of Sc for Mg and Fe for Mn will result in a FM compound. The synthesis and characterization of the $Sc_2FeRh_5B_2$ compound confirmed the prediction. Similarly, the study presented two quinternaries based on the same crystalline framework $Sc_2FeRu_3Rh_2B_2$ and $Sc_2MnRu_3Rh_2B_2$ that they computed to be AFM and confirmed experimentally afterward [126].

The same group turned to the study of the Fe_4N-based phases due to their interest as high-density recording materials. Fe_4N exhibits a large permanent magnetization, a low coercitivity (i.e., only a low-magnetic field is required to switch off the permanent magnetization) and chemical inertness. They investigated the MFe_3N compounds (with M = Fe, Co, Ni, Ru, Rh, Pd, Os, Ir, Pt) formed by the substitution of one Fe site on the Fe_4N structure. First, the stability of the different phases versus decomposition to other products (i.e., M, Fe, and FeN) was studied. The theoretical results agreed very well with previous experimental knowledge, predicting negative enthalpies of formation for all known MFe_3N compounds (i.e., M = Ni, Pd, Pt, Fe) and also led to predicting that the (previously unknown) rhodium-based compound should be stable and ferromagnetic [127]. Synthesis and magnetic characterization confirmed the existence and ferromagnetic nature of the previously unknown Rh-based compound [128]. The experimental value for the magnetic saturation per formula unit is 8.3 μ_B and in good agreement with the predicted 9.2 μ_B. Moreover, later experimental work on purer samples demonstrated that the site occupancy (in the Fe_4N structure) favored according to DFT was indeed observed experimentally [129].

While not directly opening up to immediate applications, both of these examples show that the magnetic nature of compounds can be predicted and somehow chemically tuned even before synthesis. It also represents a case in which an entirely new phase ($RhFe_3N$) was predicted through ab initio stability analysis and confirmed experimentally.

Large magnetic anisotropy in FeCo alloys In another study involving magnetism, Burkert and co-workers computationally designed an alloy with two desired properties: high magnetic-anisotropy and -saturation. As the recording density of hard disks is increasing, the magnetic energy per grain (K_uV, where K_u is the magnetic anisotropy and V is the volume of the grain) is getting small enough that thermal fluctuations could erase recorded information. Finding materials with high magnetic anisotropy can mitigate this detrimental effect. However, the required field to write on the magnetic storage device (H_w) increases with the magnetic anisotropy:

$$H_w \approx \frac{K_u}{M_s} \tag{10}$$

with M_s representing the magnetic saturation (i.e., the maximum permanent magnetization achievable). This

leads to the additional requirement of high-magnetic saturation to keep the writing field low enough.

Motivated by these design rules, the researchers computed through DFT the K_u and M_s parameters for the body centered tetragonal $Fe_{1-x}Co_x$ alloy as a function of the Co concentration (x) and the lattice parameters (c/a ratio) [130]. Figure 9 shows the results of this investigation and points out that a maximum of K_u is computed to be achievable at c/a around 1.2 and a Co concentration of 60 %. The magnetic saturation, while not maximum, is still reasonably large at 2 μ_B/atom (compared to other materials candidates, e.g., FePt) in the optimal conditions for anisotropy. To obtain this optimal c/a ratio, the material would need to be kept under strain, for instance through epitaxy.

Several follow-up experiments on different substrates (Rh, Pt, and Pt–$Fe_{1-x}Co_x$ superlattices) confirmed the exceptionally high-magnetic anisotropy combined with good magnetic saturation [106, 131, 132]. The value of optimal c/a ratio and cobalt concentration are quantitatively remarkably close to the predictions, as well as the measured magnetic saturation (e.g., 2.4 μ_B/atom exp. vs 2.1 μ_B/atom computationally [132]). On the other hand, the magnetic anisotropy, while very large and indeed two orders of magnitude higher than in the unstrained alloy [131], was measured around 100–200 μeV/atom while computed to be 700–800 μeV/atom in bulk or 380 μeV/atom in a model Pt superlattice. Recently, subsequent computations showed that the reason for this discrepancy does not lie in DFT but probably in the virtual crystal approximation (VCA) model that poorly approximates the disordered nature of the experimentally grown thin films [133].

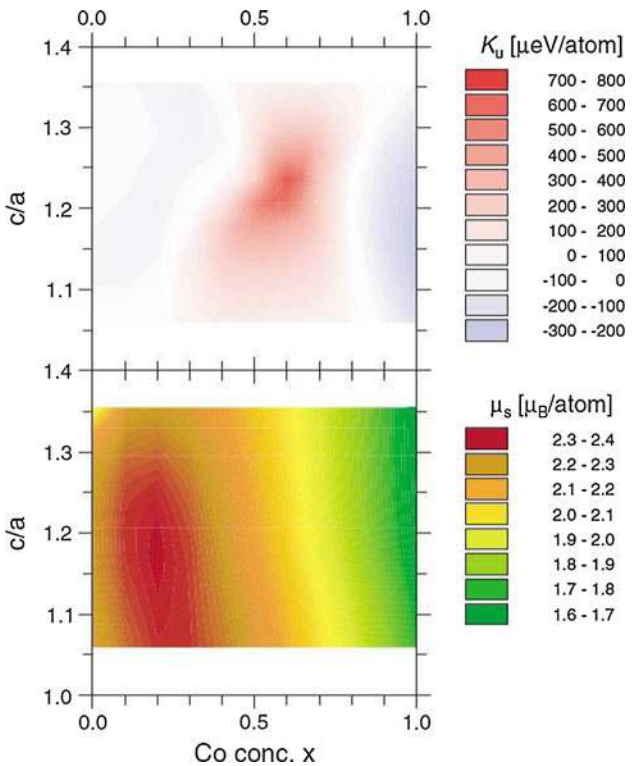

Fig. 9 Computed magnetic anisotropy (K_u) and saturation (μ_s) for $Fe_{1-x}Co_x$ as function of the concentration of Co (x) and the c/a ratio of the tetragonal crystal structure [130]. This graph was used to identify a region of c/a and x where the magnetic anisotropy is especially high. Reprinted figure with permission from [130]. Copyright 2004 by the American Physical Society

Here, it is the precise control provided by computational studies which was extremely valuable. A purely experimental study of the magnetic properties of those alloys under different strain and Co content would have been extremely time-consuming and cumbersome.

Large tunneling magneto-resistance in Fe/MgO/Fe junctions Another magnetic effect of great interest from an application point of view is tunneling magneto-resistance (TMR). When two magnetic materials are separated by a very thin insulating layer (typically a few nanometers) in a thin film sandwich structure, the electrons can tunnel through the insulating layer; the tendency to tunnel will depend on the relative electron spin alignment in the two magnetic layers. The tunneling will be facilitated when the spins are pointing in the same direction and more difficult when spins are anti-aligned. As the electron spin population in each magnetic layer can be independently controlled by external fields, the resistance of the structure, which is related to the tendency for electrons to tunnel, can be tuned magnetically. This opens the way to a control of the resistance of a device through transversal magnetic fields which is of great interest application-wise.

The TMR effect is often reported by the magnitude of the TMR coefficient, which describes the change in resistivity between the situation when the spins are in the same and opposite directions. The first measurements of the TMR effect showed a small TMR coefficient (on the order of 10–20 % at 4.2 K for a Pb/Ge/Pb structure [134]). In practice, the TMR effect could be much larger and two independent computational papers predicted that structure based on Fe/MgO/Fe should exhibit the needed high TMR effect (up to 1000 % in one of the studies) [135, 136].

One of the first measurements of thin film structures similar to the predictions (Fe/MgO/FeCo) found a TMR coefficient of 27 % at room temperature (and 60 % at 30 K) [137]. A few years later, Yusa et al. and Parkin et al. measured high TMR at room temperature on Fe/MgO/Fe structures (up to 200 %) as shown in Fig. 10 [138, 139]. In addition, the paper from Yusa confirmed the proposed theoretical mechanism based on a coherent tunneling mechanism. The difference between these two results and

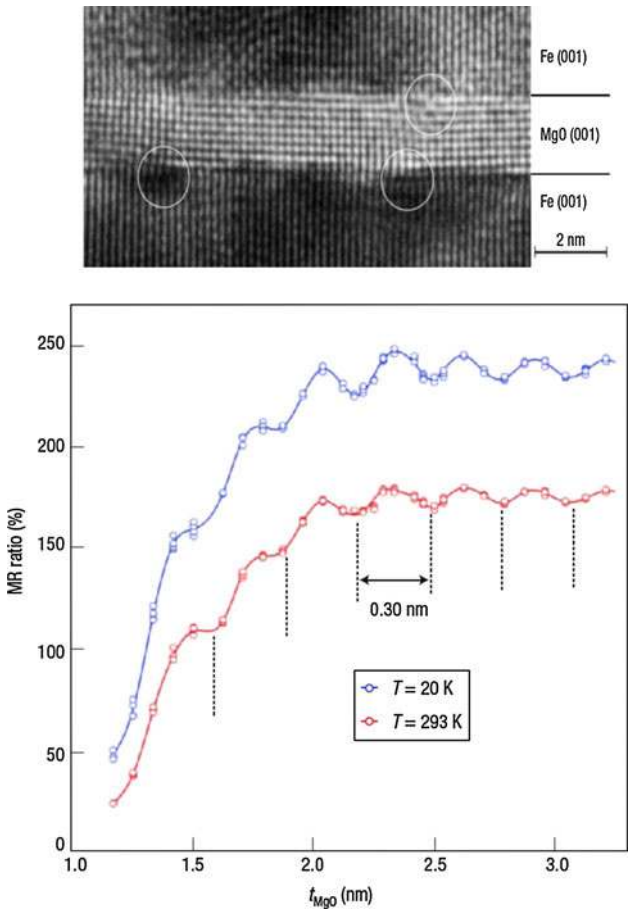

Fig. 10 High-resolution transmission electronic microscope picture of a Fe/MgO/Fe junction (the *circles* indicate disclocations) and TMR coefficient measurements in function of the MgO layer thickness [138]. The experimental measurement confirmed the very high TMR coefficient suggested by computations. Reprinted by permission from MacMillan Publishers Ltd: Nature Materials [138], copyright 2004

previous ones on MgO-based junctions is likely to come from the quality of the grown films.

This example of ab initio prediction is very close to current applications as films using this large TMR effect are already used in hard disk heads nowadays as well as in new magnetic random access memory (MRAM) chips providing non-volatile, fast and energy efficient information storage. It illustrates how computations can sometimes demonstrate the theoretical potential of a material or device that has not been achieved yet due to process limitations.

Magnetoelectric multiferroics

Another important field of research in functional materials relates to magnetoelectric multiferroics. These materials combine ferromagnetism (persistent magnetization induced by a magnetic field) with ferroelectricity (i.e., persistent electric polarization induced by an electric field). Materials combining those two properties are of interest in future device applications, especially for their possible coupling between magnetic and electric effects. For instance, a magnetoelectric material could have its magnetization controlled by an electric field and therefore lead to data storage mechanisms where the reading process is magnetic while the writing is electric, which is advantageous technologically [140, 141]. Magnetoelectric materials are, however, quite rare because ferromagnetism requires species with partially filled *d*-orbitals (e.g., Mn^{3+}, Fe^{3+}, or Ni^{2+}), while the most common form of ferroelectricity relies on the presence of species with empty *d*-orbitals (e.g., Ti^{4+}) often on B sites of a perovskite structure.

$BiMnO_3$ as a magnetoelectric multiferroics There exists, however, another mechanism for ferroelectricity requiring the displacement of species with active lone pairs (e.g., Pb^{2+} or Bi^{3+}) opening the potential to be combined with magnetic elements to form magnetoelectric multifferroics [142, 143]. In search of such a magneto-electric material, Hill and Rabe [144] computationally predicted that a known ferromagnetic material $BiMnO_3$ forming in the perovskite structure (see Fig. 11a) should also exhibit ferroelectricity. The computational study of the phonon modes indicated that one of the unstable modes indeed produced an opposite displacement of Bi and O atoms (see Fig. 11b) and led to ferroelectric behavior.

A few years later, the prediction of ferroelectricity in $BiMnO_3$ was confirmed experimentally [145]. Ferromagnetic behavior was measured (as previously known) with a Curie temperature of 105 K (see Fig. 11c), and a polarization-electric field hysteresis (see Fig. 11d), which is a signature of ferroelectricity, was observed down to 80 K, indicating that $BiMnO_3$ is, at low temperature, a magnetoelectric multiferroic. Further experimental studies confirmed these first measurements on purer samples [146].

While an early and convincing success of computational materials design, $BiMnO_3$ turned out to not have a strong enough coupling between ferroelectricity and magnetism to be of interest technologically and the quest for magnetoelectric multiferroics with strong coupling is still open and significantly driven by ab initio techniques [147].

$Ba_{0.5}Eu_{0.5}TiO_3$ as a multiferroics for the permanent electron dipole measurement The computational design of multiferroic materials is even impacting the field of theoretical physics as shown by the recent development of devices for the detection of the electron permanent dipole, the existence of which is of great importance in fundamental physics. One way of measuring the electron permanent electric dipole would be to apply an electric field on a population of electrons in a material, thereby splitting the population into two groups: one with the electric moment parallel to the field and another with the electric

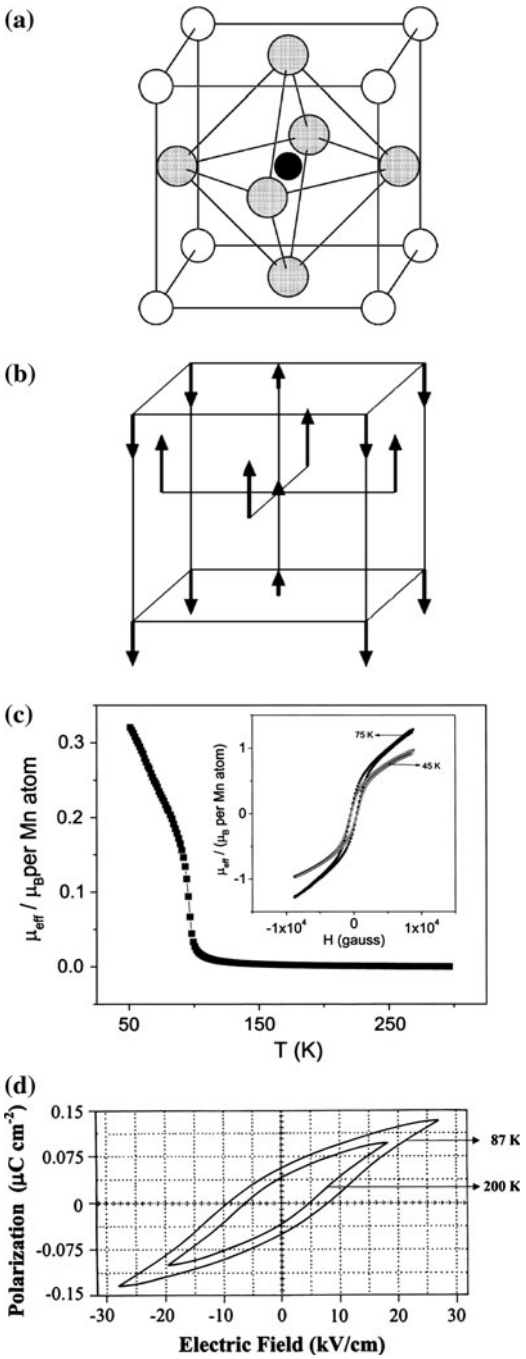

Fig. 11 **a** The perovskite structure of $BiMnO_3$. Oxygen atoms are *gray*, Mn is *black*, and Bi is *white* [144]. **b** The Eigenvectors for one of the unstable gamma point phonon modes obtained through first-principles computations [144]. The opposite displacement of Bi and O create the possibility for ferroelectricity. **c** Measurements of the magnetic saturation at low temperature and **d** polarization versus electric field at 87 and 200 K [145]. Those measurements demonstrate the coexistence of ferromagnetism and ferroelectricity at low temperature. Reprinted Figure **a** and **b** with permission from [144]. Copyright 1999 by the American Physical Society. Figure **c** and **d** are reprinted from [145], copyright 2002, with permission from Elsevier

moment anti-parallel. As physical laws impose that the spin needs to be parallel or anti-parallel to the dipole, there needs to be a net magnetization due to the electron population splitting. Measuring the change in magnetization during the reversing of the electric field could be used to deduce the electron permanent dipole.

The materials requirements to perform such an experiment are extremely severe [148]. The material needs to be ferroelectric with a large and easily switchable electric polarization at low temperature, have a high concentration of heavy ions with local magnetic moments remaining paramagnetic at low temperature (i.e., no magnetic long-range ordering), and exhibit a strong perturbation of the local environment of the magnetic ions during the ferroelectric switching. While obtaining a magnetoelectric material can be achieved at low temperature as shown in the example of $BiMnO_3$, one of the major challenges is to find a material that will not have any magnetic ordering at low temperature while conserving a high concentration of magnetic ions.

Ruschanskii et al. [148] proposed an alloy of $BaTiO_3$ and $EuTiO_3$ (both stable in a perovskite structure) as a material candidate at the $Ba_{0.5}Eu_{0.5}TiO_3$ composition. They computed that the material would exhibit ferroelectricity (through Ti^{4+}) while the magnetic Eu atoms would move significantly during the Ti off-centering in the octahedron as required. Moreover, they showed, by computing the energetics of different Ba and Eu orderings, that the Eu atoms should not interact at a long-range because of the dilution effect of the barium atoms. The synthesis and characterization of the material confirmed the computational findings [148].

The sensitivity obtained for this new material is already an order of magnitude better than previous solid-state-based measurement devices and optimization is under way. This example is typical of how computations can help solve the multi-parameter optimization problem often faced by materials scientists.

Electronic materials

First-principles computations readily provide band structures of solids. While DFT band structures have tremendously aided the understanding of many solids, there are fundamental limitations with standard DFT methods (in the GGA and LDA approximations) when quantitatively modeling the electronic structure of materials and especially their band gaps (see "Ab initio methods"). As the two following examples of carbon and boron nitride nanotubes illustrate, useful predictions can however be made when DFT is used with full knowledge of its limits

and good quantitative agreement can even be reached when more advanced techniques such as GW are used.

The electronic structure of carbon nanotubes The electronic properties of carbon nanotubes (CNT) have been of great interest for the scientific community. However, it is quite challenging to directly measure electronic properties of individual nanotubes and computations provide a much easier access to the study of CNTs electronic properties. In pioneering studies dating back to 1992, Mintmire et al. and Saito et al. [149, 150] used both DFT and tight-binding models to predict how chirality (i.e., the way the graphene sheet is folded to form the nanotube) and tube diameter influence its electronic structure. These computational predictions were confirmed a few years later through careful scanning tunneling microscopy (STM) experiments [151].

The electronic structure of boron nitride nanotubes Owing to the similarity of boron and nitrogen to carbon, a theoretical paper by Rubio et al. proposed the existence of Boron Nitride nanotubes (BNNT) and computed their electronic structures within DFT [152]. A follow-up computational study showed that to the contrary of CNTs, BNNTs should always be semiconducting and their band gaps should not depend on their chirality and diameter [153]. Soon after, the synthesis of BNNTs was demonstrated [154], and a series of measurements on single and multi-wall nanotubes confirmed the absence of correlations between chirality, diameter and band gaps [155–157]. The reported experimental (from multi-walls up to single walls nanotubes) band gap values from 4.5 to 5.8 eV are in good agreement with the computed GW value of 5.5 eV.

BNNTs have also been predicted to exhibit a large and measurable effect of a transversal electric field on the band gap of the nanotube [158]. This effect is called the giant Stark effect in reference to the Stark effect involving the splitting of energy levels of atoms or molecules in an electric field. This effect was predicted to be much larger for BNNTs than CNNTs, and is of interest in nanoelectronics because tuning the electronic properties of a nanotube with a transversal electric field could lead to interesting devices. The presence of a giant Stark effect in BNNTs was confirmed experimentally after its prediction [159].

Both these examples show the added value of first-principles predictions in fields such as nanotechnology where measurements can be extremely challenging and time-consuming.

Catalysis

Catalysts are an integral component in the production of most industrially important chemicals and in many areas of environment science. It is therefore no surprise that computational materials science techniques have been brought to bear on various aspects of surface science and catalysis, providing many qualitative and quantitative insights into experimental observations. In this section, we will focus only on examples where computational investigations have led directly to new materials. We will not discuss the significant body of computational research that have provided insights into existing catalytic phenomenon without leading directly to new materials, and will instead point the reader to other excellent reviews on this subject [160, 161].

Catalysts are generally classified as homogeneous catalysts (where the catalyst is in the same phase as the reactants) or heterogeneous catalysts (where the catalyst is in a different phase from the reactants). Given that homogeneous catalysis typically takes place in solution, most examples of computational catalyst design are for solid-state heterogeneous catalysts, which are more amenable to treatment with current first-principles methods.

A fundamental concept in catalyst design is the Sabatier principle, which states that the interaction between a catalyst and the reactants should be neither too strong nor too weak [162]. If the interaction is too weak, the reactants will fail to bind to the catalyst and no reaction will take place. On the other hand, if the interaction is too strong, the catalyst gets blocked by reactants or products that fail to dissociate. This principle leads to the now-ubiquitous "volcano" plot, where the reaction rate plotted against a property such as the heat of adsorption or binding energy of the reactant by the catalyst shows a maximum at an intermediate value for the binding energy. An example is shown in Fig. 12. The heat of adsorption or binding energy is a property that can be readily computed via DFT computations, and indeed, many early works in computational catalyst design were primarily focused on computing trends in binding energies of reactant molecules on various transition metal surfaces.

However, catalyst design, like most materials design problems, requires multi-property optimization. Besides having a reactant binding energy in the right range, a commercially viable catalyst must also satisfy fundamental criteria of selectivity, reasonable cost, ability to operate in the presence of potential poisons, and stability in the reaction media, among others. In recent years, more sophisticated approaches have been developed to computationally evaluate a large number of potential catalysts across multiple criteria.

We have divided our review on computational catalyst design into two broad categories: (i) catalysts for industrial chemical production and (ii) catalysts relating to the production and activation of hydrogen, which are key to enabling a hydrogen economy.

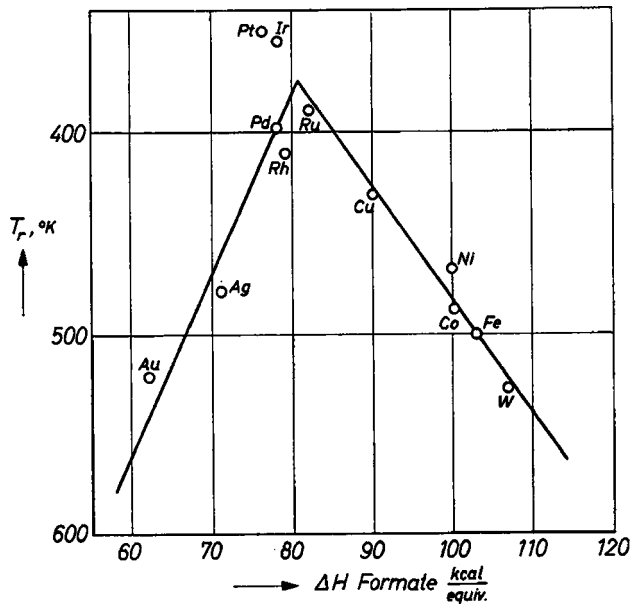

Fig. 12 Volcano plot for the relation between catalytic activity and heat of formation of the formates on various metal surfaces [163]. Peak catalytic activity is observed at an intermediate heat of formation (Sabatier Principle)

Catalysts for production of industrial chemicals

Selective hydrogenation of acetylene through Ni–Zn alloys Ethylene (C_2H_4) is the most produced organic compound in the world. It is used in the production of polyethylene, the world's most widely used plastic, and is a precursor to the manufacture of many important chemicals and polymers via oxidation, halogenation, and other reactions.

In order for ethylene to be used in the production of polymers, it must contain less than a few ppm of acetylene (C_2H_2). To achieve this, hydrogenation of acetylene ($C_2H_2 + H_2 \rightarrow C_2H_4$) is carried out commercially to selectively remove acetylene from ethylene. The most common industrially used catalyst is Pd modified by Ag, which is expensive.

Using DFT calculations, Studt et al. [164] identified Ni–Zn catalysts as cheap replacements for Pd. A selective catalyst for the hydrogenation of acetylene should have an activation barrier of ethylene that is greater than the barrier of desorption of ethylene, while still insuring a sufficiently exothermic acetylene adsorption. Studt et al. identified a scaling relation between the heats of adsorption for ethylene and acetylene and the adsorption energies of methyl molecules on a number of transition metal surfaces, from which they predicted NiZn and $NiZn_3$ to have good selectivity for acetylene hydrogenation. They also synthesised a series of Ni–Zn alloy catalysts on $MgAl_2O_4$ spinel supports with Zn content between 45 and 75 %. The experiments showed that the Ni–Zn catalyst with the highest Zn content has a selectivity better than that of even the traditional Pd–Ag catalyst, at a fraction of the materials cost.

Catalysts for production and activation of H_2

The hydrogen economy is a proposed system of delivering energy via hydrogen gas. Proponents of the hydrogen economy argue that hydrogen is an environmentally cleaner source of energy, without the release of pollutants or carbon dioxide at the point of end use as in the current hydrocarbon economy. The hydrogen economy aside, hydrogen gas itself is also an important industrial chemical, with the two largest uses being fossil fuel processing (e.g., hydrocracking) and production of ammonia. For these reasons, finding better catalysts for H_2 production and activation has been an area of active research, but it is only in the last ten years or so that computational design of such catalysts have come to the fore.

Ni–Au catalyst for steam reforming One of the earliest examples of computational catalyst design is in the area of steam reforming. Steam reforming is the most economical way of producing hydrogen and is used in the commercial bulk production of H_2. In steam reforming, hydrocarbons such as methane are converted to CO and H_2 ($CH_4 + H_2O \rightarrow CO + 3\,H_2$), typically over nickel catalysts.

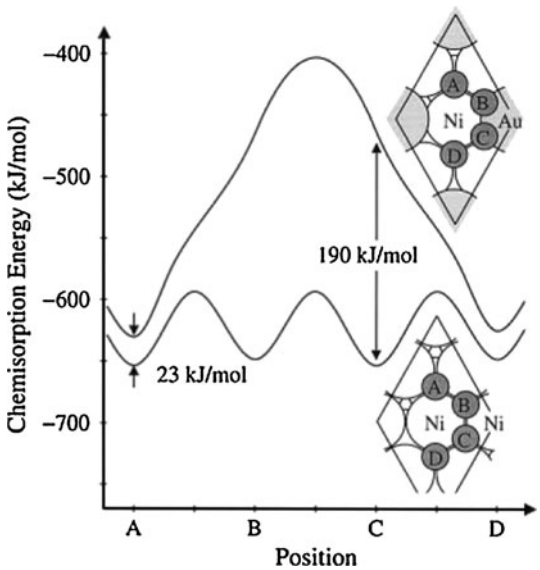

Fig. 13 Calculated adsorption energy of a C atom on a Ni(111) surface as a function of position along the surface. *Top curve* The same energy function is shown when one of the surface Ni atoms has been exchanged for a Au atom. The *insets* show the geometry in each of the two cases [165]. The presence of Au significantly lowers the adsorption energy for C. From [165], reprinted with permission from AAAS

However, nickel catalysts also catalyze the formation of graphite, which inhibits the activity of the catalyst.

In 1998, Besenbacher et al. [165] demonstrated using DFT calculations that doping a Ni catalyst with Au on the surface led to significantly lower binding energies for graphite on the surface, with only a marginal impact on methane dissociation. They calculated the adsorption energy of a C atom on a Ni(111) surface as a function of position along the surface (see Fig. 13), and found that the sites neighboring a gold atom have significantly lower C adsorption energies. Hence, even though Au alloying has been known to lead to lower CH_4 activity [166], the effect on C adsorption is far greater, making for a less reactive, but more robust, steam-reforming catalyst than pure Ni. Besenbacher et al. [165] subsequently verified these predictions via experimental synthesis, characterization and tests of a high-surface area gold–nickel catalyst.

Preferential oxidation of CO on bimetallic core–shell nanoparticles Computational catalyst design has also been applied to other limitations in the production of clean H_2 for proton exchange membrane fuel cells (PEMFCs). The reformate from industrial production of H_2 contains significant amounts of CO, which poisons the surface of the anode catalyst used in fuel cells. Typically, CO is removed from the reformate using a two-stage process: (1) water-gas shift (WGS) reaction and (2) preferential oxidation (PROX) of CO. The latter reduces the CO content of reformate down to the ppm levels needed for stable operation of PEMFCs.

Recently, Nilekar et al. [167] reported the first-principles-guided design, synthesis, and characterization of core–shell nanoparticle (NP) catalysts made of a transition metal core covered with a $\approx$1–2 monolayer-thick shell of Pt atoms for preferential CO oxidation in hydrogen-rich environments (PROX). Nilekar et al. used DFT calculations to determine the binding energy of CO on M@Pt surfaces, which is directly related to the difficulty of removing CO from the surface through either oxidation or desorption, and showed that improvements in PROX activity of Pt monolayers on various supporting metals are directly related to weakening of the CO binding energy. Ru@Pt was found to have the lowest binding energy for CO among the M@Pt surfaces investigated, and hence had the most facile removal of CO. Nilekar et al. also performed experiments to validate the first-principles results, and confirmed that Ru@Pt core–shell NPs show the highest PROX reactivity among the M@Pt NPs investigated and are also more active than their constituent pure metal NPs as well as conventional nano alloys.

H_2 activation with Ti-doped Al One of the key commercial barriers to adoption of hydrogen-based energy is that the catalysts are typically based on expensive noble metals (e.g., Pt, Pd, Rh). In two papers [168, 169], Chaudhuri and Chopra et al. demonstrated that aluminum doped with very small amounts of Ti can activate molecular H_2 at temperatures as low as 90 K. In the earlier work, Chaudhuri et al. showed using first-principles techniques that a particular local arrangement of Ti atoms is responsible for catalyzing the chemisorption of molecular hydrogen on Ti–Al surfaces. The subsequent work by Chopra et al. published 6 years later extended the earlier first-principles calculations. By using CO as a probe molecule to identify the atomic arrangement of the catalytically active sites containing Ti on the Al(111) surfaces, Chopra et al. provided direct experimental evidence of that Ti-doped Al can perform the first step of molecular hydrogen activation under nearly barrierless condition .

BiPt as a new hydrogen evolution reaction catalyst Besides the industrial processes of steam reforming, hydrogen can also be produced via water-splitting, and the key reaction in the process is known as the hydrogen evolution or HER (Eq. 11).

$$2H^+ + 2e \rightarrow H_2 \tag{11}$$

In two seminal works published in 2007 [170, 171], Greeley et al. outlined a scheme for the screening of heterogeneous catalysts using DFT, with a particularly successful demonstration of its application to HER catalyst design. Their screening approach involves not only an evaluation of the surface activity for the reaction, but also includes several assessments for stability in real electrochemical environments. The evaluation of surface activity is based on the well-established atomic-scale descriptor for catalytic activity, i.e., a plot of the HER catalytic activity of a metal against hydrogen-metal bond strength show a volcano relationship. Greeley et al. also developed four tests of the stability of the catalyst in real-world environment: (i) free-energy change associated with surface segregation events; (ii) free-energy change associated with intrasurface transformations such as island formation and surface de-alloying; (iii) free energy of oxygen adsorption, beginning with splitting of liquid water (related to surface poisoning and oxide formation); and (iv) free energies of dissolution as a measure of corrosion resistance.

By applying the above screening approach to 256 pure metals and surface alloys (see Fig. 14), Greeley et al. identified several surface alloys as potentially interesting for the HER. From Fig. 14, it is evident that many alloys are predicted to have free energies of hydrogen-adsorption (ΔG_H) similar to pure Pt, suggesting they would have a high-predicted HER activity. However, only a small fraction of these alloys are predicted to be both active and

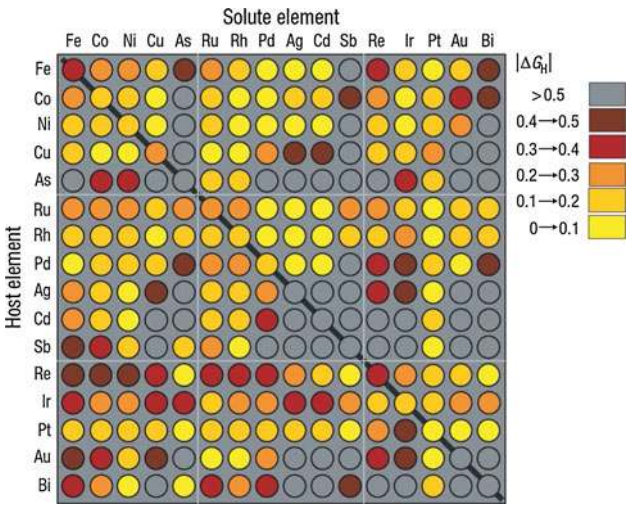

Fig. 14 Computational high-throughput screening for ΔG_H on 256 pure metals and surface alloys [170]. The *rows* indicate the pure metal substrates, and the *columns* indicate the solute embedded in the surface layer of the substrate. The solute coverage and adsorbed hydrogen coverage are 1/3ML in all cases. The diagonal of the plot corresponds to the hydrogen-adsorption free energy on the pure metal surfaces. It can be observed that many alloys have an energy of H_2 adsorption similar to pure Pt and hence are predicted to have high-predicted HER activity. Reprinted by permission from MacMillan Publishers Ltd: Nature Materials [170], copyright 2006

stable in acidic HER environments, demonstrating the importance of stability considerations in finding realistic catalysts. In the study, Greeley et al. selected the BiPt alloy for further investigation as it is one of the alloys that shows both high HER activity and good stability. The fact that BiPt is predicted to have high activity is surprising given that Bi itself is known to be a poor electrocatalyst for the HER. Nonetheless, subsequent synthesis of this BiPt surface alloy showed that it does indeed have comparable activity with pure Pt, validating the effectiveness of the screening approach. This result is a particularly effective demonstration of the power of computational materials design, which enabled the discovery of a catalyst (BiPt) that might otherwise not have been found based on conventional chemical intuition.

Status, challenges, and future of computational materials discovery and design

During the last few decades, first-principles computations have been used extensively to understand and rationalize the properties of materials, offering essential insight into materials behavior at the atomistic level. Nowadays, as envisioned by a few pioneers [172–174], the field is turning more and more toward performing bolder predictions, driving experimental studies with a real potential to accelerate new materials design. In this review, we focused on a few case studies where computational predictions were made and confirmed experimentally afterwards and illustrated the status of *in silico* materials design, showing the successes but also the limitations and future challenges in the field.

At first, computational materials design might be thought of as a process involving the computations of all properties governing a material's behavior. However, in practice, this is far from being the case as the final behavior of a material also depends on factors that are difficult to compute. For instance, the quality of a hydrogen storage material such as $LiNH_2$–MgH_2 (1:1) was found to not depend only on the easily computable thermodynamics of the system but also on process route such as the ball-milling procedure.

The dependence of a material's overall behavior on properties that are not easily computable is sometimes considered as a major limitation to computational material design, and many efforts are currently directed toward improving the computational techniques and the fundamental understanding of many physical phenomena to increase the range of computable properties. However, in practice, there is no need to "compute everything", and the computational approach can provide enough necessary but not sufficient conditions to perform an important screening before in-depth experimental work is performed. For example, even though important properties for battery materials such as cyclability are difficult to directly predict, a Li-ion battery cathode material without an adequate computed voltage, thermodynamic stability, and Li-ion diffusion can be excluded from consideration application-wise. The power of computational predictions rely here in its potential for narrowing down the list of often time-expensive experiments to perform.

Interestingly, while computationally driven materials discovery is often thought of as a very quantitative approach, it sometimes also relies on qualitative observations. For instance, it is possible to make predictions simply by looking at specific features in the electronic structure, as illustrated by example of the high-thermopower $FeSb_2$. Besides qualitative results, ab initio computations often rely on their ability to effectively rank materials properties. For instance, even though a calculated adsorption energy on a catalyst might not be quantitatively accurate, what often matters for experimental guidance is to know the top candidates within a set of potential materials. For some properties, fully quantitative results can be obtained. Examples from our review include voltage in the Li-ion battery examples, reaction energy for the $LiNH_2$–MgH_2 hydrogen storage material, magnetic moments in the nitrides, borides, and FeCo alloy cases, and band gaps in the example of boron nitride nanotubes. However, one should always keep in mind the inherent accuracy of the

method that has been used. Sometimes, it is difficult to estimate the accuracy of a particular DFT property computation over broad chemical spaces that encompass many types of materials, and the establishment of unbiased statistical comparisons between computed and experimental values will become more and more important as the field is getting more predictive.

It is still rare to predict an entirely new phase of matter with interesting technological properties, and our case study list included only a few entirely novel compounds. However, we believe that the recent developments in compound and crystal-structure prediction will make the computational discovery of entirely novel phase more common in the future. Even when computations identify phases likely to be stable, the exact way of synthesizing the novel inorganic compound is still often a trial-and-error process depending a lot on the solid-state chemist experience and skills. In some cases computations can provide some guidance toward possible synthesis routes, as illustrated by the Na–Li ion-exchange route for synthesizing $Li_3M(CO_3)(PO_4)$, but a better theoretical understanding of the factors controlling inorganic solid synthesis would dramatically help the materials discovery process.

Even when studying known phases of matter, computations can be extremely valuable in helping to identify compounds with rare properties (e.g., the magnetoelectricity in $BiMnO_3$) or push to the reinvestigation of a compound that in retrospect is obviously interesting but got lost in the experimental process (e.g., monoclinic $LiMnBO_3$ cathode). The history of materials science is full of compounds that were known but had unknown unusual properties, such as the MgB_2 superconductor [175], and computations will be a future catalyst for the identification of those hidden gems. Computational studies also often provide insight into the type of perturbation required to improve a known system (e.g., aluminum doping in $LiCoO_2$ will increase the voltage or Au alloying in Ni will lower carbon poisoning of steam-reforming catalysts). Finally, by providing theoretical limits to a specific property, the computational approach can also help identify the potential of new material not achieved yet due for instance to process limitations, and rationally point out situations in which efforts in process optimization might be rewarding. For instance, the theoretical prediction of large TMR effect in Fe/MgO/Fe was probably one of the driving force for process optimization of these structures.

Our review focused on computational predictions that have been confirmed experimentally, but first-principles computations are also extremely valuable in identifying "negative results" and indicating the inherent limit to certain approaches and chemistries. For instance, Greeley et al. applied a high-throughput screening approach for finding binary alloys with good oxygen reduction reaction (ORR) capability [176]. The approach was similar to the one we reported on hydrogen reduction catalysts that identified BiPt, but they found here that while many alloys have high-predicted activity for the ORR, almost all are predicted to be unstable at the high potentials associated with the ORR. Though this study did not identify a specific material of interest, it has helped exclude a large space of materials and redirected efforts for ORR catalysts to focus on other promising approaches. Similarly, a large-scale computational study of phosphates as cathode material not only identified novel compounds such as $Li_9V_3(P_2O_7)_3(PO_4)_2$, but also showed some of the limits inherent to the phosphate chemistry in terms of volumetric energy density, voltage range, and safety [177].

As ab initio software is getting more user friendly and computational resources available to research groups are increasing, we are experiencing an emerging approach consisting of high-throughput computational studies. In this approach, properties are computed for thousands of potential materials candidates, scanning the chemical space with a speed difficult to achieve experimentally [41, 178, 179]. This review already presented many examples of materials discovered through high-throughput computing (e.g., LiZnSb in thermoelectrics, BiPt in catalysis, a few new cathode materials in Li-ion batteries and a specific mixture of $LiNH_2$–MgH_2 in hydrogen storage). High-throughput computing studies have already been performed in numerous fields such as catalysis [170], hydrogen storage [180], Li-ion batteries [181, 182], organic photovoltaics [183], thermoelectrics [114, 184], scintillators [185, 186], or photocatalysts [187]. In parallel, this large amount of computed properties is getting compiled in databases publicly available through web interfaces as the *Materials Project* and others [188–190]. By providing access to computed databases to the whole scientific community, experimentalists and theorists alike, we are convinced those public databases will facilitate future computationally driven materials discovery.

Conclusion

In this review, we surveyed a number of applications for which first-principles techniques have guided successful experimental results. For many of the examples, calculations motivated reinvestigation of known compounds that might have otherwise remained overlooked for technological applications. In others, a new material was essentially predicted and designed completely *in silico*. These pioneering studies demonstrate that ab initio calculations are now capable of not only characterizing known compounds but in many cases driving experimental studies toward materials of technological interest.

As this review illustrated, many of the tools already available are capable of driving materials design. However, the field of first-principles computations is rapidly evolving, and expected future advancements include more accurate treatments of exchange/correlation and excited-state properties, improved numerical algorithms for performing DFT calculations and structure prediction, cheaper and more powerful computational resources, frameworks for high-throughput calculation, and comprehensive public databases of calculated materials properties.

We are confident that currently available as well as future methodologies will lead to many more technological materials having their origin in computational predictions.

Acknowledgements Geoffroy Hautier acknowledges the F.R.S.-FNRS Belgium for financial support under a "Chargé de Recherche" grant. Anubhav Jain acknowledges funding through the U.S. Government under Contract DE-AC02-05CH11231 and the Luis W. Alvarez Fellowship in Computational Science. The authors would like also to strongly acknowledge the many experts who were kind enough to share their thoughts and experience in materials design: Gerbrand Ceder, Jean-Christophe Charlier, Ralf Drautz, Richard Dronskowski, Olle Eriksson, Jeffrey Greeley, Xavier Gonze, Karl Johnson, Aleksey Kolmogorov, Georg Madsen, Jeff Neaton, and Nicola Spaldin.

References

1. Eagar TW (1995) Technol Rev 98(2)
2. Hohenberg P, Kohn W (1964) Phys Rev 136:B864
3. ABINIT. http://www.abinit.org/. Accessed 15 March 2012
4. Vienna Ab Initio Simulation Package (VASP). http://www.vasp.at/. Accessed 15 March 2012
5. Quantum Espresso. http://www.quantum-espresso.org/. Accessed 15 March 2012
6. Hafner J (2000) Acta Mater 48(1):71
7. Hafner J, Wolverton C, Ceder G (2006) MRS Bull 31(9):659
8. Martin RM (2004) In: Electronic structure: basic theory and practical methods, vol 1. Cambridge University Press, New York
9. Burke K (2003) The ABC of DFT. http://dft.uci.edu/sites/default/files/g1.pdf. Accessed 15 March 2012
10. Argaman N, Makov G (2000) Am J Phys 68(1):69
11. Carter EA (2008) Science 321(5890):800
12. Kohn W, Sham LJ (1965) Phys Rev 140:A1133
13. Perdew JP, Burke K, Ernzerhof M (1996) Phys Rev Lett 77(18):3865
14. Perdew JP, Parr RG, Levy M, Balduz JL (1982) Phys Rev Lett 49:1691
15. Jonsson H, Mills G, Jacobsen KW (1998) In: Nudged elastic band method for finding minimum energy paths of transitions. World Scientific Publishing Co. Pte. Ltd., Singapore
16. Mills G, Jónsson H (1994) Phys Rev Lett 72(7):1124
17. Anisimov VI, Aryasetiawan F, Lichtenstein AI (1997) J Phys: Condens Matter 9:767
18. Zhou F, Cococcioni M, Kang K, Ceder G (2004) Electrochem Commun 6:1144
19. Cococcioni M, de Gironcoli S (2005) Phys Rev B 71:035105
20. Wang L, Maxisch T, Ceder G (2006) Phys Rev B 73(19):195107
21. Wang L, Maxisch T, Ceder G (2007) Chem Mater 19(3):543
22. Heyd J, Scuseria GE, Ernzerhof M (2006) J Chem Phys 124(21):219906
23. Heyd J, Scuseria GE, Ernzerhof M (2003) J Chem Phys 118(18):8207
24. Heyd J, Scuseria GE (2004) J Chem Phys 121(3):1187
25. Chevrier VL, Ong SP, Armiento R, Chan MKY, Ceder G (2010) Phys Rev B 82(7):075122
26. Wang C, Pickett W (1983) Phys Rev Lett 51(7):597
27. Sham L, Schlüter M (1983) Phys Rev Lett 51(20):1888
28. Cohen A, Mori-Sánchez P, Yang W (2008) Phys Rev B 77(11):115123
29. Chan M, Ceder G (2010) Phys Rev Lett 105(19):196403
30. Hedin L (1965) Phys Rev 139(3A):A796
31. Aryasetiawan F, Gunnarsson O (1998) Rep Progr Phys 61:237
32. Runge E, Gross EKU (1984) Phys Rev Lett 52(12):997
33. Tran F, Blaha P (2009) Phys Rev Lett 102(22):5
34. Kuisma M, Ojanen J, Enkovaara J, Rantala T (2010) Phys Rev B 82(11):1
35. Gritsenko O, van Leeuwen R, van Lenthe E, Baerends E (1995) Phys Rev A 51(3):1944
36. Maddox J (1998) Nature 335:201
37. Schon JC, Doll K, Jansen M (2010) Phys Status Solidi (B) 247(1):23
38. Woodley SM, Catlow R (2008) Nat Mater 7(12):937
39. O'Keeffe M (2010) Phys Chem Chem Phys: PCCP 12: 8580. doi:10.1039/C004039H
40. Lany S (2008) Phys Rev B 78(24):1
41. Jain A, Hautier G, Moore CJ, Ping Ong S, Fischer CC, Mueller T, Persson KA, Ceder G (2011) Comput Mater Sci 50:2295
42. Jain A, Hautier G, Ong SP, Moore C, Fischer CC, Ceder G (2011) Phys Rev B 84:045115
43. Hautier G, Ong SP, Jain A, Moore CJ, Ceder G (2012) Phys Rev B 85:155208. doi:10.1103/PhysRevB.85.155208
44. Oganov AR, Valle M (2009) J Chem Phys 130(10):104504
45. Ducastelle F (1991) In: Order and phase stability in alloys, (Cohesion and Structure) , vol 3. North Holland, Amsterdam
46. Ceder G (1993) Comput Mater Sci 1(2):144
47. Sanati M, Wang L, Zunger A (2003) Phys Rev Lett 90(4):1
48. Blum V, Zunger A (2004) Phys Rev B 69(2):20103
49. Hart GLW (2009) Phys Rev B 80(1):1
50. Van Der Ven A, Aydinol MK, Ceder G (1998) J Electrochem Soc 145(6):2149
51. Wales DJ, Doye JPK (1997) J Phys Chem A 101(28):5111
52. Wales DJ, Scheraga HA (1999) Science 285(5432):1368
53. Bush TS, Catlow CRA, Battle PD (1995) J Mater Chem 5(8):1269
54. Abraham NL, Probert MIJ (2006) Phys Rev B 73(22):1
55. Oganov AR, Glass CW (2006) J Chem Phys 124(24):244704
56. Trimarchi G, Zunger A (2007) Phys Rev B 75(10):1
57. Oganov AR, Glass CW (2006) J Phys: Condens Matter 20(6):064210
58. Zhang X, Zunger A, Trimarchi G (2010) J Chem Phys 133(19):194504
59. Oganov AR, Chen J, Gatti C, Ma Y, Ma Y, Glass CW, Liu Z, Yu T, Kurakevych OO, Solozhenko VL (2009) Nature 457(February):863. doi:10.1038/nature07736
60. Kolmogorov A, Shah S, Margine E, Bialon A, Hammerschmidt T, Drautz R (2010) Phys Rev Lett 105(21):1
61. Ono S, Kikegawa T, Ohishi Y (2007) Am Miner 92(7):1246
62. Liebold-Ribeiro Y, Fischer D, Jansen M (2008) Angew Chem Int Ed 47(23):4428 (in English)
63. Johnson DC (2008) Nature 454(7201):174
64. Ceder G, Morgan D, Fischer C, Tibbetts K, Curtarolo S (2006) MRS Bull 31(12):981
65. Curtarolo S, Morgan D, Persson K, Rodgers J, Ceder G (2003) Phys Rev Lett 91(13):1

66. Fischer CC, Tibbetts KJ, Morgan D, Ceder G (2006) Nat Mater 5(8):641
67. Hautier G, Fischer C, Ehrlacher V, Jain A, Ceder G (2011) Inorg Chem 50:656
68. Kolmogorov AN, Curtarolo S (2006) Phys Rev B 74(22):1
69. Kolmogorov AN, Curtarolo S (2006) Phys Rev B 73(18):1
70. Levy O, Chepulskii RV, Hart GLW, Curtarolo S (2009) J Am Chem Soc 29: 163
71. Hautier G, Fischer CC, Jain A, Mueller T, Ceder G (2010) Chem Mater 22:3762
72. http://ceder.mit.edu/ternaryoxides. Accessed 15 March 2012
73. Fix T, Sahonta SL, Garcia V, MacManus-Driscoll JL, Blamire MG (2011) Cryst Growth Des 11 (5): 1422
74. Uratani Y, Shishidou T, Oguchi T (2008) Jpn J Appl Phys 47(9):7735
75. Matar S, Baraille I, Subramanian M (2009) Chem Phys 355(1):43
76. http://han.ess.sunysb.edu/∼USPEX/. Accessed 15 March 2012
77. http://www.maise-guide.org/. Accessed 15 March 2012
78. http://www.materialsproject.org/apps/structure_predictor. Accessed 15 March 2012
79. Wadia C, Alivisatos AP, Kammen DM (2009) Environ Sci Technol 43(6):2072
80. Wadia C, Albertus P, Srinivasan V (2011) J Power Sour 196(3):1593
81. Jaramillo P, Samaras C, Wakeley H, Meisterling K (2009) Energy Policy 37(7):2689
82. ISuppli IHS (2011) IHS iSuppli Rechargeable Battery Special Report. Tech. rep.
83. Aydinol M, Kohan A, Ceder G, Cho K, Joannopoulos J (1997) Phys Rev B 56(3):1354
84. Maxisch T, Zhou F, Ceder G (2006) Phys Rev B 73(10):1
85. Morgan D, Van Der Ven A, Ceder G (2004) Electrochem Solid-State Lett 7(2):A30
86. Ong SP, Jain A, Hautier G, Kang B, Ceder G (2010) Electrochem Commun 4:1
87. Ceder G, Hautier G, Jain A, Ong S (2011) MRS Bull 36(03):185
88. Meng YS, Arroyo-de Dompablo ME (2009) Energy Environ Sci 2(6):589
89. Ceder G (2010) MRS Bull 35(September):693. doi:10.1557/mrs2010.681
90. Ceder G, Chiang YM, Sadoway D, Aydinol M, Jang YI, Huang B (1998) Nature 392(6677):694
91. Kang K, Meng YS, Bréger J, Grey CP, Ceder G (2006) Science 311(5763):977
92. Chen H, Hautier G, Jain A, Moore C, Kang B, Doe R, Wu L, Zhu Y, Tang Y, Ceder G (2012, submitted)
93. Legagneur V (2001) Solid State Ion 139(1–2):37
94. Kim JC, Moore CJ, Kang B, Hautier G, Jain A, Ceder G (2011) J Electrochem Soc 158(3):A309
95. Ceder G, Kim JC, Kang B, Moore CJ, Hautier G (2011) International Patent Application PCT/US2011/035432
96. Ceder G, Jain A, Hautier G, Kim JC, Kang BW (2010) US Patent Application 12/857262
97. Kuang Q, Xu J, Zhao Y, Chen X, Chen L (2011) Electrochim Acta 56(5):2201
98. Kuang Q, Lin Z, Zhao Y, Chen X, Chen L (2011) J Mater Chem 3:2
99. Jain A, Hautier G, Moore CJ, Kang B, Lee J, Chen H, Twu N, Ceder G (2012) J Electrochem Soc 159(5):A622
100. Hautier G, Jain A, Chen H, Moore C, Ong SP, Ceder G (2011) J Mater Chem 21:17147
101. Ceder G, Chen H, Doe RE, Hautier G, Jain A, Kang B (2011) International patent application pct/us2011/025684
102. Crabtree GW, Dresselhaus MS (2008) MRS Bull 33(4):421
103. Wolverton C, Siegel DJ, Akbarzadeh aR, Ozoliš V (2008) J Phys: Condens Matter 20(6):064228
104. Ozolins V, Akbarzadeh aR, Gunaydin H, Michel K, Wolverton C, Majzoub EH (2009) J Phys: Conf Ser 180:012076
105. Alapati SV, Johnson JK, Sholl DS (2006) J Phys Chem B 110(17):8769
106. Lu J, Fang Z, Choi Y, Sohn H (2007) J Phys Chem C 111(32):12129
107. Luo W (2004) J Alloys Compd 381(1–2):284
108. Osborn W, Markmaitree T, Shaw LL (2007) J Power Sour 172(1):376
109. Liu Y, Zhong K, Gao M, Wang J, Pan H, Wang Q (2008) System 2(6):3521
110. Lu J, Choi YJ, Fang ZZ, Sohn HY (2010) J Power Sour 195(7):1992
111. Tritt TM, Böttner H, Chen L (2008) MRS Bull 33(4):366
112. Tritt T, Subramanian M (2006) MRS Bull 31(03):188
113. Chen G, Dresselhaus MS, Dresselhaus G, Fleurial JP, Caillat T (2003) Int Mater Rev 48(1):45
114. Madsen GKH(2006) J Am Chem Soc 128(37):12140
115. Bergerhoff G, Hundt R, Sievers R, Brown I (1983) J Chem Inf Comput Sci 23(2):66
116. Inorganic Crystal Structure Database. http://www.fiz-karlsruhe.de/icsd.html. Accessed 15 March 2012
117. Toberer ES, May AF, Scanlon CJ, Snyder GJ (2009) J Appl Phys 105(6):063701
118. Van De Walle CG, Neugebauer J (2004) J Appl Phys 95(8):3851
119. Lany S, Zunger A (2008) Phys Rev B 78(23):17
120. Madsen GKH, Bentien A, Johnsen S, Iversen BB (2005) In: Proceedings of the 24th International Conference on Thermoelectrics, vol. 8328. IEEE, New York
121. Petrovic C, Lee Y, Vogt T, Lazarov N, Budko S, Canfield P (2005) Phys Rev B 72(4):1
122. Bentien A, Madsen G, Johnsen S, Iversen B (2006) Phys Rev B 74(20):2
123. Bentien A, Johnsen S, Madsen GKH, Iversen BB, Steglich F (2007) Europhys Lett (EPL) 80(1):17008
124. Comstock R (2002) J Mater Sci: Mater Electron 13(9):509
125. Spaldin NA (2010) Magnetic materials: fundamentals and applications. Cambridge University Press
126. Dronskowski R, Korczak K, Lueken H, Jung W (2002) Angew Chem Int Ed 41(14):2528 (in English)
127. von Appen J, Dronskowski R (2005) Angew Chem Int Ed 44(8):1205 (in English)
128. Houben A, Müller P, von Appen J, Lueken H, Niewa R, Dronskowski R (2005) Angew Chem Int Ed 44(44):7212 (in English)
129. Houben A, Sepelak V, Becker KD, Dronskowski R (2009) Chem Mater 21:784
130. Burkert T, Nordström L, Eriksson O, Heinonen O (2004) Phys Rev Lett 93(2):1
131. Winkelmann A, Przybylski M, Luo F, Shi Y, Barthel J (2006) Phys Rev Lett 96(25):1
132. Andersson G, Burkert T, Warnicke P, Björck M, Sanyal B, Chacon C, Zlotea C, Nordström L, Nordblad P, Eriksson O (2006) Phys Rev Lett 96(3):1
133. Neise C, Schönecker S, Richter M, Koepernik K, Eschrig H (2011) Phys Status Solidi (B) 248(10):2398
134. Julliere M (1975) Phys Lett A 54(3):225
135. Mathon J, Umerski A (2001) Phys Rev B 63(22):1
136. Butler W, Zhang XG, Schulthess T, MacLaren J (2001) Phys Rev B 63(5):1
137. Bowen M, Cros V, Petroff F, Fert A, Martnez Boubeta C, Costa-Kramer JL, Anguita JV, Cebollada A, Briones F, de Teresa JM, Morellon L, Ibarra MR, Guell F, Peiro F, Cornet A (2001) Appl Phys Lett 79(11):1655

138. Yuasa S, Nagahama T, Fukushima A, Suzuki Y, Ando K (2004) Nat Mater 3(12):868
139. Parkin SSP, Kaiser C, Panchula A, Rice PM, Hughes B, Samant M, Yang SH (2004) Nat Mater 3(12):862
140. Spaldin Na, Fiebig M (2005) Science 309(5733):391
141. Eerenstein W, Mathur ND, Scott JF (2006) Nature 442(7104): 759
142. Hill N (2000) J Phys Chem B 104(29):6694
143. Ederer C, Spaldin NA (2005) Curr Opin Solid State Mater Sci 9(3):128
144. Hill N, Rabe K (1999) Phys Rev B 59(13):8759
145. Moreira dos Santos A (2002) Solid State Commun 122:49
146. Kimura T, Kawamoto S, Yamada I, Azuma M, Takano M, Tokura Y (2003) Phys Rev B 67(18):2
147. Cheong SW, Mostovoy M (2007) Nat Mater 6(1):13
148. Rushchanskii KZ, Kamba S, Goian V, Vanek P, Savinov M, Prokleska J, Nuzhnyy D, Knízek K, Laufek F, Eckel S, Lamoreaux SK, Sushkov aO, Lezaić M, Spaldin Na (2010) Nat Mater 9(8):649
149. Mintmire J, Dunlap B (1992) Phys Rev Lett 68(5):631
150. Saito R, Fujita M, Dresselhaus G, Dresselhaus MS (1992) Appl Phys Lett 60(18):2204
151. Wildoer J, Venema L, Rinzler A, Smalley R (1998) Nature 584(10):59
152. Rubio A, Corkill J, Cohen M (1994) Phys Rev B, Condens Matter 49(7):5081
153. Blase X, Rubio A, Louie S (1994) Europhys Lett 28: 335
154. Chopra NG, Luyken RJ, Cherrey K, Crespi VH, Cohen ML, Louie SG, Zettl A (1995) Science 269(5226):966
155. Fuentes G, Borowiak-Palen E, Pichler T, Liu X, Graff A, Behr G, Kalenczuk R, Knupfer M, Fink J (2003) Phys Rev B 67(3):1
156. Czerw R, Webster S, Carroll DL, Vieira SMC, Birkett PR, Rego CA, Roth S (2003) Appl Phys Lett 83(8):1617
157. Arenal R, Stéphan O, Kociak M, Taverna D, Loiseau A, Colliex C (2005) Phys Rev Lett 95(12):1
158. Khoo K, Mazzoni M, Louie S (2004) Phys Rev B 69(20):1
159. Ishigami M, Sau J, Aloni S, Cohen M, Zettl A (2005) Phys Rev Lett 94(5):1
160. Greeley J, Nørskov JK, Mavrikakis M (2002) Ann Rev Phys Chem 53:319
161. Nørskov JK, Abild-Pedersen F, Studt F, Bligaard T (2011) Proc Nat Acad Sci USA 108(3):937
162. Deutschmann O, Knözinger H, Kochloefl K, Turek T (2011) In: Ullmann's Encyclopedia of industrial chemistry. Wiley-VCH Verlag GmbH & Co. KGaA, Weinheim
163. Rootsaert WJM, Sachtler WMH (1960) Zeitschrift Physik Chem 26(1–2):16
164. Studt F, Abild-Pedersen F, Bligaard T, Sørensen RZ, Christensen CH, Nørskov JK (2011) Science 320:1320
165. Besenbacher F (1998) Science 279(5358):1913
166. Kratzer P, Hammer B, Nørskov JK (1996) J Chem Phys 105(13): 5595
167. Nilekar AU, Alayoglu S, Eichhorn B, Mavrikakis M (2010) J Am Chem Soc 2:7418
168. Chaudhuri S, Muckerman JT (2005) J Phys Chem B 109(15): 6952
169. Chopra IS, Chaudhuri S, Veyan JF, Chabal YJ (2011) Nat Mater 10(11):884
170. Greeley J, Jaramillo TF, Bonde J, Chorkendorff IB, Nørskov JK (2006) Nat Mater 5(11):909
171. Greeley J, Nørskov JK (2007) Surf Sci 601(6):1590
172. Cohen M (1994) Solid State Commun 92(1–2):45
173. Zunger A (1998) Curr Opin Solid State Mater Sci 3(1):32
174. Ceder G (1998) Science 280(5366):1099
175. Nagamatsu J, Nakagawa N, Muranaka T, Zenitani Y, Akimitsu J (2001) Nature 410(6824):63. doi:10.1038/35065039
176. Greeley J, Nørskov JK (2009) J Phys Chem C 113(12):4932
177. Hautier G, Jain A, Ong SP, Kang B, Moore C, Doe R, Ceder G (2011) Chem Mater 23:3495
178. Munter TR, Landis DD, Abild-Pedersen F, Jones G, Wang S, Bligaard T (2009) Comput Sci Discov 2(1):015006
179. Setyawan W, Curtarolo S (2010) Comput Mater Sci 49(2):299
180. Hummelshøj JS, Landis DD, Voss J, Jiang T, Tekin A, Bork N, Duak M, Mortensen JJ, Adamska L, Andersin J, Baran JD, Barmparis GD, Bell F, Bezanilla AL, Bjork J, Björketun ME, Bleken F, Buchter F, Bürkle M, Burton PD, Buus BB, Calborean A, Calle-Vallejo F, Casolo S, Chandler BD, Chi DH, Czekaj I, Datta S, Datye A, DeLaRiva A, Despoja V, Dobrin S, Engelund M, Ferrighi L, Frondelius P, Fu Q, Fuentes A, Fürst J, García-Fuente A, Gavnholt J, Goeke R, Gudmundsdottir S, Hammond KD, Hansen HA, Hibbitts D, Hobi E, Howalt JG, Hruby SL, Huth A, Isaeva L, Jelic J, Jensen IJT, Kacprzak KA, Kelkkanen A, Kelsey D, Kesanakurthi DS, Kleis J, Klüpfel PJ, Konstantinov I, Korytar R, Koskinen P, Krishna C, Kunkes E, Larsen AH, Lastra JMG, Lin H, Lopez-Acevedo O, Mantega M, Martínez JI, Mesa IN, Mowbray DJ, Mýrdal JSG, Natanzon Y, Nistor A, Olsen T, Park H, Pedroza LS, Petzold V, Plaisance C, Rasmussen JA, Ren H, Rizzi M, Ronco AS, Rostgaard C, Saadi S, Salguero LA, Santos EJG, Schoenhalz AL, Shen J, Smedemand M, Stausholm-Møller OJ, Stibius M, Strange M, Su HB, Temel B, Toftelund A, Tripkovic V, Vanin M, Viswanathan V, Vojvodic A, Wang S, Wellendorff J, Thygesen KS, Rossmeisl J, Bligaard T, Jacobsen KW, Nørskov JK, Vegge T (2009) J Chem Phys 131(1):014101
181. Hautier G, Jain A, Ong SP, Kang B, Moore C, Doe R, Ceder G (2011) Chem Mater 23:3495
182. Mueller T, Hautier G, Jain A, Ceder G (2011) Chem Mater 23:3854
183. Olivares-Amaya R, Amador-Bedolla C, Hachmann J, Atahan-Evrenk S, Sánchez-Carrera RS, Vogt L, Aspuru-Guzik A (2011) Energy Environ Sci 4:4849
184. Wang S, Wang Z, Setyawan W, Mingo N, Curtarolo S (2011) Phys Rev X 1(2):1
185. Ortiz C, Eriksson O, Klintenberg M (2009) Comput Mater Sci 44(4):1042
186. Setyawan W, Gaume RM, Lam S, Feigelson RS, Curtarolo S (2011) ACS Comb Sci 13(4): 382
187. Castelli IE, Olsen T, Datta S, Landis DD, Dahl Sr, Thygesen KS, Jacobsen KW (2012) Energy Environ Sci 5: 5814. doi: 10.1039/C1EE02717D
188. http://www.materialsproject.org. Accessed 15 March 2012
189. http://www.aflowlib.org. Accessed 15 March 2012
190. http://gurka.fysik.uu.se/ESP/. Accessed 15 March 2012